

THE AGE SPREAD OF QUIESCENT GALAXIES WITH THE NEWFIRM MEDIUM-BAND SURVEY: IDENTIFICATION OF THE OLDEST GALAXIES OUT TO $Z \sim 2$

KATHERINE E. WHITAKER^{1,2}, PIETER G. VAN DOKKUM^{1,2}, GABRIEL BRAMMER^{1,2}, MARISKA KRIEK^{3,2}, MARIJN FRANX⁴, IVO LABBÉ^{5,2}, DANILO MARCHESINI^{6,2}, RYAN F. QUADRI^{4,2}, RACHEL BEZANSON¹, GARTH D. ILLINGWORTH⁷, KYOUNG-SOO LEE¹, ADAM MUZZIN^{1,2}, GREGORY RUDNICK^{8,2}, DAVID A. WAKE¹

Accepted for publication in the Astrophysical Journal

ABSTRACT

With a complete, mass-selected sample of quiescent galaxies from the NEWFIRM Medium-Band Survey (NMBS), we study the stellar populations of the oldest and most massive galaxies ($>10^{11} M_{\odot}$) to high redshift. The sample includes 570 quiescent galaxies selected based on their extinction-corrected $U-V$ colors out to $z=2.2$, with accurate photometric redshifts, $\sigma_z/(1+z) \sim 2\%$, and rest-frame colors, $\sigma_{U-V} \sim 0.06$ mag. We measure an increase in the intrinsic scatter of the rest-frame $U-V$ colors of quiescent galaxies with redshift. This scatter in color arises from the spread in ages of the quiescent galaxies, where we see both relatively quiescent red, old galaxies and quiescent blue, younger galaxies towards higher redshift. The trends between color and age are consistent with the observed composite rest-frame spectral energy distributions (SEDs) of these galaxies. The composite SEDs of the reddest and bluest quiescent galaxies are fundamentally different, with remarkably well-defined 4000Å- and Balmer-breaks, respectively. Some of the quiescent galaxies may be up to 4 times older than the average age- and up to the age of the universe, if the assumption of solar metallicity is correct. By matching the scatter predicted by models that include growth of the red sequence by the transformation of blue galaxies to the observed intrinsic scatter, the data indicate that most early-type galaxies formed their stars at high redshift with a burst of star formation prior to migrating to the red sequence. The observed $U-V$ color evolution with redshift is weaker than passive evolution predicts; possible mechanisms to slow the color evolution include increasing amounts of dust in quiescent galaxies towards higher redshift, red mergers at $z \lesssim 1$, and a frosting of relatively young stars from star formation at later times.

Subject headings: cosmology: observations – galaxies: evolution – galaxies: formation

1. INTRODUCTION

Massive galaxies with strongly suppressed star formation exist out to and beyond a redshift of $z \sim 2$ (e.g. Labbé et al. 2005; Daddi et al. 2005; Kriek et al. 2006, 2009; Fontana et al. 2009), and these red, quiescent galaxies form well-defined color-mass and color-magnitude relations (CMR), known as the red sequence (e.g. Kriek et al. 2008). The scatter in the color of red sequence galaxies provides a natural marker for the variation in star formation histories. Galaxies with stellar populations that formed at different epochs will have an intrinsic scatter in their colors, and this scatter will decrease as these red sequence galaxies evolve.

In simple models, the scatter in the observed color of

red sequence galaxies increases with redshift as the fractional age differences between the galaxies becomes larger (Bower et al. 1992; Ellis et al. 1997; van Dokkum et al. 1998). In more complex models that include morphological transformations, the scatter can be constant or even decrease with redshift (van Dokkum & Franx 2001; Romeo et al. 2008). Directly probing the scatter in color (as well as the scatter in age) as a function of redshift will constrain these models.

The intrinsic scatter in the $U-V$ colors of local early-type galaxies in the Coma Cluster is ~ 0.03 mag (Bower et al. 1992). Most of the work at higher redshifts has been done only in clusters, finding a roughly constant internal $U-V$ scatter of $\sim 0.08 \pm 0.03$ mag at $0.05 < z < 0.8$, increasing to ~ 0.15 at $z=1.6$ (van Dokkum et al. 2000; Holden et al. 2004; McIntosh et al. 2005b; Lidman et al. 2008; Mei et al. 2009; Ruhland et al. 2009; Hilton et al. 2009; Papovich et al. 2010). To date, there are no measurements of the intrinsic scatter in the CMR for field galaxies at $z \gtrsim 1$, because this requires accurate rest-frame colors and methods of separating star-forming and quiescent galaxies.

At high redshift, the color-mass relation is “diluted” by dusty star-forming galaxies, and the dust complicates the measurements of the intrinsic color scatter of red, old galaxies. This complication is less important at low redshift because $\sim 70-80\%$ of red galaxies have very little dust (Bell et al. 2004a; Wolf et al. 2005). Furthermore, dusty contaminants can be visually identified using mor-

katherine.whitaker@yale.edu

¹ Department of Astronomy, Yale University, New Haven, CT 06511

² Visiting Astronomer, Kitt Peak National Observatory, National Optical Astronomy Observatory, which is operated by the Associations of Universities for Research in Astronomy (AURA) under cooperative agreement with the National Science Foundation.

³ Department of Astrophysical Sciences, Princeton University, Princeton, NJ 08544

⁴ Sterrewacht Leiden, Leiden University, NL-2300 RA Leiden, The Netherlands

⁵ Carnegie Observatories, Pasadena, CA 91101

⁶ Department of Physics and Astronomy, Tufts University, Medford, MA 02155

⁷ UCO/Lick Observatory, Pasadena, CA 91101

⁸ Department of Physics and Astronomy, University of Kansas, Lawrence, KS 66045

phological information out to $z \sim 1$ (e.g. McIntosh et al. 2005a; Ruhland et al. 2009), whereas at higher redshifts the galaxies are too faint to resolve with current technology. However, these dusty systems can be identified using additional information: e.g. UVJ rest-frame colors (Williams et al. 2009), the visual dust extinction from SED modeling (Brammer et al. 2009), or mid-IR imaging (Papovich et al. 2005; Franx et al. 2008; Fontana et al. 2009).

Currently the best estimates for the ages of stellar populations in massive high redshift galaxies comes from Kriek et al. (2008), who combine broadband multiwavelength imaging with NIR spectroscopy for a K -selected sample. They find that red sequence galaxies at $z \sim 2.3$ typically have 0.5-1 Gyr populations with moderate amounts of dust. However, older galaxies may have been missed due to the magnitude limits of the K -selection. To understand the properties of quiescent galaxies, a large systematic study is required to connect and confirm the limited knowledge we have of galaxies at $z \sim 2$ with the observed properties of local early-type galaxies.

High redshift studies of galaxies are either based on small, accurate spectroscopic samples that are biased due to the methods of selection, or large photometric samples limited by the accuracy of the photometric redshifts and depth of the survey. To address the problems associated with each method, the NEWFIRM Medium-Band Survey (NMBS, van Dokkum et al. 2009) was designed to improve the photometric redshift accuracies while maintaining a large sample of galaxies. For the first time, we are able to determine the color scatter of galaxies on the red sequence for a complete, mass-selected sample with accurate photometric redshifts.

In this paper, we study the properties of a mass-selected sample of galaxies from the NMBS over four redshift intervals, focusing on the properties of the quiescent galaxies residing on the red sequence. Here, we will use the term “quiescent” to signify old stellar populations with red rest-frame colors ($U-V \gtrsim 1.4$) that are not vigorously forming stars. Following Brammer et al. (2009), we correct the rest-frame $U-V$ colors for dust reddening allowing a clean separation of the red and blue sequences. As expected, the star formation rates of these “quiescent” galaxies from SED modeling are typically low (the median SFR is $0.2 M_{\odot} \text{ yr}^{-1}$), although some probably have ongoing star formation up to the level of $\sim 10 M_{\odot} \text{ yr}^{-1}$. Probing the internal scatter for the first time at $z \gtrsim 1$, we show trends of $U-V$ color with the relative ages of the stellar populations and the composite rest-frame spectral energy distributions (SEDs) of all quiescent galaxies. We show that the results would be similar if we used the UVJ color selection of Williams et al. (2009). Finally, we place constraints on the star formation histories for passive evolution given the observed intrinsic scatter as a function of redshift.

We assume a Λ CDM cosmology with $\Omega_M=0.3$, $\Omega_{\Lambda}=0.7$, and $H_0=70 \text{ km s}^{-1} \text{ Mpc}^{-1}$ throughout the paper. All magnitudes are given in the AB system.

2. DATA

The NEWFIRM Medium-Band Survey (NMBS) employs a new technique of using medium-bandwidth near-IR filters to sample the Balmer/4000Å break from 1.5 <

$z < 3.5$ at a higher resolution than the standard broadband near-IR filters (van Dokkum et al. 2009), thereby improving the accuracy of the photometric redshifts. We briefly summarize the survey here, the full details of the reduction, source detection, and generation of the photometric catalogs will be described in K.E. Whitaker et al. (*in prep*). The NMBS survey is based on a similar concept to the optical medium-band filters used in the COMBO-17 survey (Wolf et al. 2003). A custom set of five medium bandwidth filters in the wavelength range of 1-1.7 μm were manufactured for the NEWFIRM camera on the Kitt Peak 4m telescope for the survey. Data were taken over the 2008A, 2008B, and 2009A semesters, with a total of 75 nights (45 nights through the NOAO Survey Program and an additional 30 nights through a Yale-NOAO time trade).

The survey targets two $\sim 0.25 \text{ deg}^2$ fields within the Cosmological Evolution Survey (COSMOS) and All-wavelength Extended Groth Strip International Survey (AEGIS), chosen to take advantage of the wealth of publically-available ancillary data over a broad wavelength range. We combine our five medium-band near-IR images and a broad-band K -band image taken with the NEWFIRM camera with optical images in the $ugriz$ broad-band filters of both survey fields, made publically available through the CFHT Legacy Survey⁹, using images reduced by the CARS team (Erben et al. 2009; Hildebrandt et al. 2009). Additionally, we include deep Subaru images with the $B_J V_J r^+ i^+ z^+$ broad-band filters in the COSMOS field (Capak et al. 2007). Finally, we include IR images in the *Spitzer*-IRAC bands over the entire COSMOS pointing that are provided by the S-COSMOS survey (Sanders et al. 2007), and partial coverage of the AEGIS pointing ($\sim 0.15 \text{ deg}^2$) overlapping with the Extended Groth Strip (Barmby et al. 2008).

In this study, we use a K -selected catalog generated from the 2008A and 2008B semesters only. The AEGIS catalog contains 15 filters and the COSMOS catalog contains 21 filters ($u-8\mu\text{m}$). The optical and near-IR images were convolved to the same point-spread function (PSF) before performing aperture photometry, so as to limit any bandpass-dependent effects. The photometry was done with SExtractor (Bertin & Arnouts 1996) in relatively small circle apertures chosen to optimize the signal-to-noise. We determine an additional aperture correction from the K -band image that accounts for flux that falls outside of the AUTO aperture, thereby enabling us to calculate total magnitudes (see, e.g. Labbé et al. 2003). We use an alternative source fitting algorithm especially suited for heavily confused images for which a higher resolution prior (in this case, the K -band image) is available to extract the photometry from the IRAC images¹⁰. This method is described in more detail in the appendix of Marchesini et al. (2009).

Using the EAZY photometric redshift and rest-frame color code (Brammer et al. 2008), we find the photometric redshifts in COSMOS to be in excellent agreement

⁹ <http://www.cfht.hawaii.edu/Science/CFHTLS/>

¹⁰ Through visual inspections of the residual IRAC images (after subtracting the modeled K-detected objects), we estimate that flux contributions from undetected K-band sources may influence the IRAC photometry for less than 5% of the entire quiescent sample studied in this work at a level greater than the formal error bars.

with the spectroscopic redshifts made publically available through the z COSMOS survey (Lilly et al. 2007), with $\sigma_z/(1+z)=0.016$ for 632 objects at $z_{\text{spec}} < 1$. We also find excellent agreement between the photometric and spectroscopic redshifts for a larger sample of 2313 objects at $z_{\text{spec}} < 1.5$ in AEGIS from the DEEP2 survey (Davis et al. 2003) with $\sigma_z/(1+z)=0.017$. Both fields have very few catastrophic failures, with only 3% $>5\sigma$ outliers. Spectroscopic redshifts also exist for 125 Lyman Break Galaxies (LBGs) at $z \sim 3$ within the AEGIS field from Steidel et al. (2003), for which we find $\sigma_z/(1+z)=0.045$, with 10% $>5\sigma$ outliers. However, we note that LBGs are very faint in the rest-frame optical (observer’s near-IR) and their spectra have relatively weak Balmer/4000Å breaks. There is excellent agreement between the NMBS photometric redshifts and the Gemini/GNIRS redshifts from Kriek et al. (2006), with a biweight scatter in $(z_{\text{phot}} - z_{\text{spec}})/(1+z_{\text{spec}})$ of only 0.010, albeit this is only for four galaxies (see van Dokkum et al. 2009). The photometric redshift accuracies range from $\sigma_z/(1+z) \sim 0.01$ for galaxies with stronger Balmer/4000Å breaks to $\sigma_z/(1+z) \sim 0.05$ for galaxies with less defined breaks. The lack of spectroscopic redshifts above $z \sim 1$ highlights the necessity for both follow-up spectroscopy at high redshift, as well as the innovation of new techniques to accurately diagnose the reliability of the photometric redshifts (see Quadri & Williams 2009).

From the best-fit EAZY template, we compute the rest-frame $U-V$ colors following the method used by Wolf et al. (2003) in the COMBO-17 survey. We measure the rest frame $U-V$ color from the best-fit template, using the filter definitions of Maíz Apellániz (2006). When using closely-spaced medium-band observed filters, the template fluxes are found to be more robust than interpolating between observed filters (see Brammer et al. *in prep*). The resulting $U-V$ colors have average uncertainties of $\sim 0.058 \pm 0.008$ mag for the entire sample of massive ($>10^{11} M_{\odot}$) galaxies, as determined from both systematic uncertainties and Monte Carlo simulations (described in detail in §3.2).

We fit the photometry with stellar population synthesis templates using FAST (Kriek et al. 2009), fixing the redshift to the EAZY output (or the spectroscopic redshift where available), and determine the best-fit age, dust extinction, star formation timescale, stellar mass, and star formation rate. The models input to FAST are a grid of Maraston (2005) models that assume a Kroupa (2001) IMF with solar metallicity and a range of ages (7.6-10.1 Gyrs), exponentially declining star formation histories ($7 < \tau < 10$ in log years) and dust extinction ($0 < A_V < 4$). The dust content is parameterized by the extinction in the V-band following the Calzetti et al. (2000) extinction law¹¹.

In this paper, we select massive ($>10^{11} M_{\odot}$) galaxies in four redshift bins from the NMBS that sample roughly equal co-moving volumes (with the exception of the lowest redshift bin). Within this sample of massive galaxies, we are interested in understanding galaxies that are on the red sequence because they have old, evolved stellar

populations. At high z , where we currently lack morphological information, we must devise a method for selection of dusty, star-forming galaxies masquerading as red, quiescent galaxies.

3. THE AGE SPREAD OF QUIESCENT GALAXIES

3.1. Selecting Quiescent Galaxies

The color-mass relation is shown in the top panels of Figure 1. Clearly, the majority of massive galaxies with masses $>10^{11} M_{\odot}$ are red at all redshifts to $z=2$. However, a significant fraction of these galaxies are red because of dust, not because they have old, evolved stellar populations (e.g. Wyder et al. 2007; Cowie & Barger 2008; Brammer et al. 2009).

Following Brammer et al. (2009), we select quiescent galaxies by requiring,

$$(U - V)' - \Delta_{UV} - (2.03 - 0.77 \cdot t_{LB}/t_H) > -0.4, \quad (1)$$

where $(U-V)'$ is the rest-frame $U-V$ color with the slope of the color-magnitude relation removed using the non-evolving slope from Bell et al. (2004b) and Δ_{UV} is dust reddening correction factor of $0.47 \cdot A_V$ (the visual extinction) as derived using the Calzetti et al. (2000) extinction law. The final term accounts for a mean linear color evolution with time, where t_{LB} is the lookback time and t_H is the Hubble time. The average selection given by Equation 1 corresponds to the dashed horizontal line at each redshift interval. The selection method removes dusty, star forming galaxies based on their extinction thereby leaving us with the red sequence. This selection is similar to and more conservative than the UVJ selection of Labbé et al. (2005) and Williams et al. (2009) (see Appendix A).

Comparing the observed $U-V$ color to the color with an additional dust-correction Δ_{UV} (top and bottom panels in Figure 1, respectively), we find that not all massive red galaxies are old, as there is a significant population of dusty and star forming massive galaxies at $z > 1$ (see Brammer et al. 2009). Those star forming galaxies that are dusty interlopers are marked as green stars in the bottom panels of Figure 1 and removed from the sample through the above selection method. Additionally, those galaxies that have MIPS detections ($>20 \mu\text{Jy}$) are indicated with small red circles, but are not removed from the sample¹²; these objects likely host active galactic nuclei (AGN) or may be forming stars (see also Daddi et al. 2007). We note that the scatter measured in $U-V$ decreases by ~ 0.03 mag at $z \sim 0.5$ and $\sim 0.01-0.02$ at higher redshifts when removing all MIPS-detected quiescent galaxies. The extinction correction effectively reduces the number of galaxies in the transition zone between the blue cloud and red sequence, revealing distinct populations with bimodal intrinsic colors up to at least $z \sim 2$.

This selection method is enabled by the increased resolution provided by the near-IR medium-bandwidth filters. The improved sampling of the SEDs enable robust constraints on both the photometric redshifts ($\sim 2\%$

¹¹ We note that different dust attenuation laws have little effect on quiescent galaxies (see Muzzin et al. 2009).

¹² 24 μm fluxes from *Spitzer*-MIPS images provided by the *S-COSMOS* and *FIDEL* surveys, see Brammer et al. (2009) for a full description.

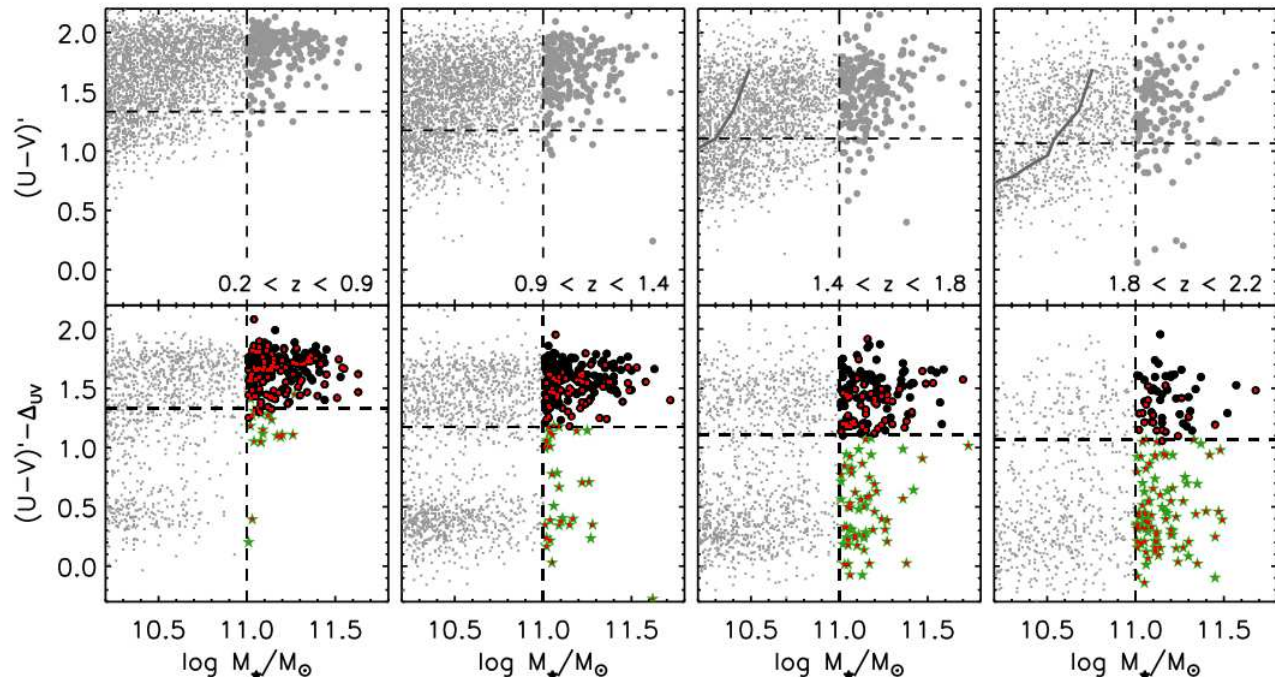


FIG. 1.— The rest-frame $U-V$ color with the slope of the CMR removed using a non-evolving slope from Bell et al. (2004b) (top panels) as well as a correction for the dust-content (bottom panels) as a function of stellar mass. Those quiescent galaxies with stellar masses $>10^{11} M_{\odot}$ on the red sequence are black, filled circles, and the dusty galaxies with obscured star formation are green stars. Small red circles indicate galaxies with MIPS detections $>20\mu\text{Jy}$. The vertical dashed lines identify the lower limit of the mass-selected sample and the horizontal dashed lines are the mean selection limits in each redshift bin. The grey lines in the top panels are the 90% completeness levels for $K_{\text{tot}} > 22.8$ ABmag at the maximum redshift of the bin. The completeness lines for $z < 1.4$ fall off the plot, with masses $< 10^{10.2} M_{\odot}$. Nearly all massive galaxies are red (top panel), but some of these galaxies have red $U-V$ colors due to dust reddening from obscured star formation. When we correct the $U-V$ colors for the amount of dust (from SED modeling), we see a bimodal color distribution at all redshifts.

accuracies compared to the $\sim 6\text{-}7\%$ accuracies of broadband z_{phot} when using all available spectroscopic redshifts) as well as the dust content of the stellar populations (see Brammer et al. 2009). The typical upper and lower 68% confidence intervals on the dust extinction (for both quiescent and star forming galaxies) range from $^{+0.3}_{-0.3}$ at $z \sim 0.5$ to $^{+0.2}_{-0.1}$ at $z \sim 2$. Furthermore, the inclusion of IRAC data helps constrain the overall shape of the SED and significantly improves the confidence intervals of the dust extinction for the individual galaxies (e.g. Labbé et al. 2005; Wuyts et al. 2007; Muzzin et al. 2009). About 20% of the quiescent galaxies have no IRAC coverage as we did not make any restrictions in our selection method, which may imply that their classification as quiescent is less robust (see, e.g., Labbé et al. 2005). We verified that these 20% of objects do not deviate systematically from the trends we see for the sample of objects with IRAC coverage. We note that this selection method is consistent with the UVJ -selection, which does not depend on models (see Appendix A.).

In Figure 2, we show two example SEDs from the highest redshift bin normalized at $1\mu\text{m}$ to highlight both the improved sampling of the SED as well as the fundamental differences between the SEDs of the quiescent and dusty galaxies. Although both galaxies have red observed $U-V$ colors, we see clear distinctions in the continuum shapes of the SEDs. The dusty galaxy (right panel) has a more gradual slope than the intrinsically red, older stellar population (left panel), which shows a well-defined 4000\AA break with a peaked SED. With the

increased resolution of the medium-band data, we are able to distinguish the continuum shapes and properties of galaxies residing on the red sequence to remove dusty contaminants such as the galaxy in the right panel.

The issue of the ongoing star-formation in these galaxies is ambiguous, as this depends on the definition of a “quiescent” galaxy and is very model-dependent: for an individual quiescent galaxy the 1σ range of specific star formation rates (sSFR) from the SED modeling described in §2 is on average 0 to 0.004 Gyr^{-1} out to $z=2$ (see also Kriek et al. 2008). Degeneracies between the age, dust, and mass in models complicate matters when selecting “quiescent” galaxies based on their sSFRs. The observational selection of quiescent galaxies in this work is less model dependent than Romeo et al. (2008) for example, who select quiescent galaxies by $\text{sSFR} < 0.01 \text{ Gyr}^{-1}$ from their simulations. About $\sim 35\%$ of our quiescent galaxies at $1.8 < z < 2.2$ appear to have sSFRs $> 0.01 \text{ Gyr}^{-1}$, with a maximum sSFR of $\sim 0.06 \text{ Gyr}^{-1}$ (as determined from SED modeling). This fraction decreases to $\sim 14\%$ by $0.2 < z < 0.9$, with a maximum sSFR of 0.02 Gyr^{-1} . A sample of quiescent galaxies selected solely on best-fit sSFR would be biased against including the blue tail of the distribution of galaxies that may be the most recent additions to the red sequence. In Appendix A, we repeat key parts of the analysis using an alternative selection of quiescent galaxies, the UVJ method of Labbé et al. (2005) and Williams et al. (2009). This method naturally isolates a distinct sequence of “red and dead” galaxies in the rest-frame $U-V$ versus $V-J$ dia-

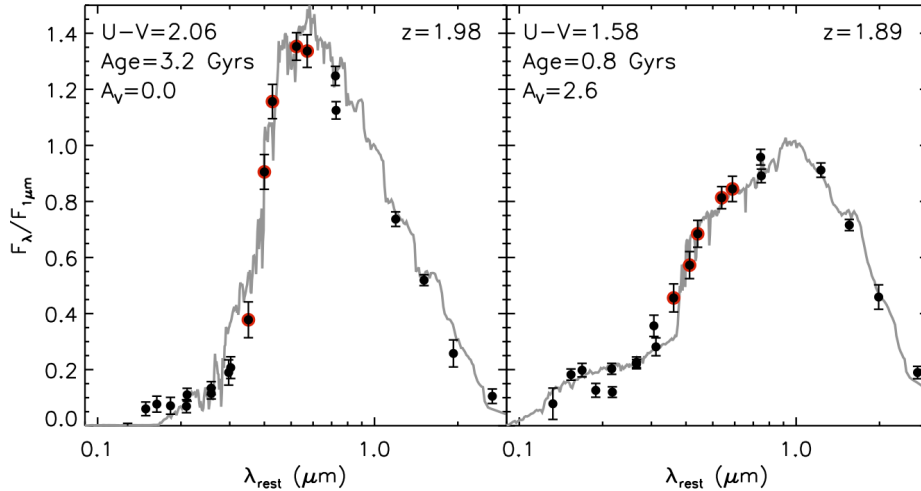


FIG. 2.— Sample SEDs normalized to $1\mu\text{m}$ from the highest redshift bin, showing the effects of increased dust content for galaxies with red observed $U-V$ colors. The red points are the medium-band filters in addition to the full $u-8\mu\text{m}$ data (black points), with the best-fit FAST template in grey. The two galaxies have similar $U-V$ colors but different amounts of dust reddening; the quiescent galaxy in the left panel has a strong 4000\AA break and a peaked SED, while the dusty galaxy in the right panel has a much more gradual slope in the Balmer-break region, rising to a peak at $\sim 1\mu\text{m}$.

gram. We find that the results remain essentially unchanged when this selection is used, but note that the UVJ selection includes a slightly higher number of blue galaxies at high redshift.

3.2. Deriving the Intrinsic Scatter in Quiescent Galaxies

In Figure 3, we show that the observed scatter in the $U-V$ color (green) increases with redshift for this sample of massive, quiescent galaxies. We note that the scatter is measured from the actual colors of the quiescent sample, not the dust-corrected colors shown in Figure 1, as there are degeneracies in the models that limit the level of accuracy of A_V . To interpret this increase we need to correct for the scatter introduced by photometric errors, thereby measuring the intrinsic scatter. For each quiescent galaxy, the observed $u-8\mu\text{m}$ fluxes were each perturbed by a normally-distributed, pseudo-random number from a Gaussian distribution with a mean of zero and a standard deviation of the photometric error for each respective filter. From these perturbed flux values, we generate 50 simulated catalogs and use EAZY to re-determine $U-V$, refitting the photometric redshifts. We take the biweight sigma of the $U-V$ distribution for each galaxy to signify the uncertainty in the color. The average uncertainty in the colors due to photometric error for all massive ($>10^{11} M_\odot$) galaxies ranges from 0.008 mag at $z=0.5$ to 0.05 mag at $z=2^{13}$.

We calculated the contribution of the photometric error to our measurement in the scatter of $U-V$ by creating a sample of mock galaxies with an intrinsic scatter of 0 (in other words, all galaxies have the same $U-V$ color). Each mock galaxy is assigned a value for the scatter in $U-V$ that comes from our simulations as described above, and we then perturb the colors by an amount that is drawn from a Gaussian distribution with width equal to the color uncertainty. The scatter of colors in the resulting

sample is then taken to be the contribution of photometric errors to the overall observed scatter. Finally, in order to reduce random uncertainties, we repeat this procedure 100 times. The contribution to the observed $U-V$ scatter from photometric error increases with z , as one might expect, from 0.007 ± 0.005 mag at $0.2 < z < 0.9$ up to 0.05 ± 0.02 mag at $1.8 < z < 2.2$, but it is significantly less than the observed color scatter at all redshifts. We note that the uncertainties in the $U-V$ colors are smaller than the observed flux error bars that sample the rest-frame U and V regions. The rest-frame U and V fluxes are typically calculated from 2-3 medium band filters, which reduces the uncertainties.

The errors in the photometry are very small at low redshift; therefore any perturbation of the fluxes does not significantly change the photometric redshift and the $U-V$ color. There are however systematic uncertainties that will contribute to the measured scatter. To assess the effects of systematic errors, we use the 75 quiescent galaxies at $0.2 < z < 0.9$ that have a spectroscopic redshift. We compared the $U-V$ colors measured for these quiescent galaxies from the photometric redshifts to the color measured using the spectroscopic redshifts. The error in redshift is strongly correlated with the resulting error in color, where an under-estimate in z_{phot} of 0.1, leads to a $U-V$ color that is ~ 0.2 mag redder (see Appendix C). The normalized median absolute deviation of $(U-V)_{\text{spec}} - (U-V)_{\text{phot}}$ is 0.05 magnitudes. We conservatively assume that the contribution to the measured scatter due to systematic uncertainties is 0.05 mag at all redshifts, but note that this may decrease at higher redshifts as our medium-band filters sample the rest-frame U and V filters at $z > 1$. The scatter in the color due to measurement error is taken to be the systematic and photometric errors added in quadrature (blue points in Figure 3).

To measure the internal scatter in $U-V$ in Figure 3 (black), we subtract the scatter due to measurement error (blue) in quadrature from the observed scatter. The vertical black error bars are the uncertainties in the me-

¹³ In Appendix B, we address the possible concern that our photometric errors have been greatly underestimated.

dian value of the photometric scatter and the horizontal black error bars are the bin size. The grey filled region indicates the range of σ_{U-V} values we measure when we raise and lower the horizontal limit in Figure 1 by 0.2 magnitudes, thereby changing the number of quiescent galaxies selected. Regardless of the selection limit, we find an increasing intrinsic scatter with redshift. We compare our measurements to work done by Bower et al. (1992) in the Coma Cluster, as well as a study of the massive ($M_{\text{dyn}} > 10^{11} M_{\odot}$) early-type galaxies in 7 clusters from $z=0.18$ to 0.84 (van Dokkum 2008). We find that the scatter at $z=0.5$ is similar to the intrinsic scatter of field galaxies recently measured by Ruhland et al. (2009)¹⁴, but a factor of 2 higher than that measured previously in clusters at these redshifts. This may reflect a systematic difference between field and cluster galaxies or some unrecognizable error contribution within our data. We note that if we limit the quiescent sample to the 75 galaxies with a spectroscopic redshift between $0.2 < z < 0.9$, we find a very similar (somewhat larger) scatter. van Dokkum & van der Marel (2007) found that the massive red sequence galaxies in clusters are typically $\sim 0.4 \pm 0.2$ Gyr older than field galaxies. If quenching in the cluster environment occurred 0.4 Gyr before quenching in the field, our models (described in §5) suggest that the intrinsic scatters should be lower by only ~ 0.02 mag, rather than the ~ 0.05 mag difference shown in Figure 3.

From Figure 3, we see that the intrinsic scatter in the colors of quiescent galaxies increases out to $z \sim 1$ and likely continues to increase to $z \sim 2$, although there may exist selection biases in this regime. It seems likely that the trend at $1 < z < 2$ is real given the recent results of Hilton et al. (2009), who measure an intrinsic z_{850-J} scatter (close to the rest-frame $U-V$) of 0.123 ± 0.049 magnitudes for a cluster at $z = 1.46$, and Papovich et al. (2010), who find $\sigma_{U-B} = 0.136 \pm 0.024$ magnitudes for a cluster at $z = 1.62$. Furthermore, the color scatter is in qualitative agreement with the predictions of simple passive evolution models that the scatter in color should decrease as the galaxies evolve.

3.3. Origin of the Intrinsic Scatter in Quiescent Galaxies

To understand the origin of the intrinsic scatter in $U-V$, we consider the properties of these stellar populations through spectral synthesis modeling. The scatter in the red sequence is thought to be determined by the scatter in both the age and metallicity, where the scatter in relative ages is generally thought to be the dominant driver (e.g. Bower et al. 1992; Gallazzi et al. 2006). The range of metallicities observed for local red sequence ellipticals from SDSS DR2 is $\sim 0.8-1.6 Z_{\odot}$ from the faintest to the brightest galaxies, with a $g-r$ color scatter of $\sim 0.04-0.05$ magnitudes (Gallazzi et al. 2006). In this work, we fix the metallicity to Z_{\odot} , but we cannot exclude that metallicity variations contribute to the scatter. We test the effects of metallicity on the scatter in $U-V$ color in Appendix E, finding a weak and opposite trend for the color scatter due to metallicity variations with redshift. Given the observed scatter in Figure 3, it is unlikely that metallicity has a large effect on this work.

¹⁴ We do not include the Ruhland et al. (2009) data in Figure 3 as that study probes a different mass range.

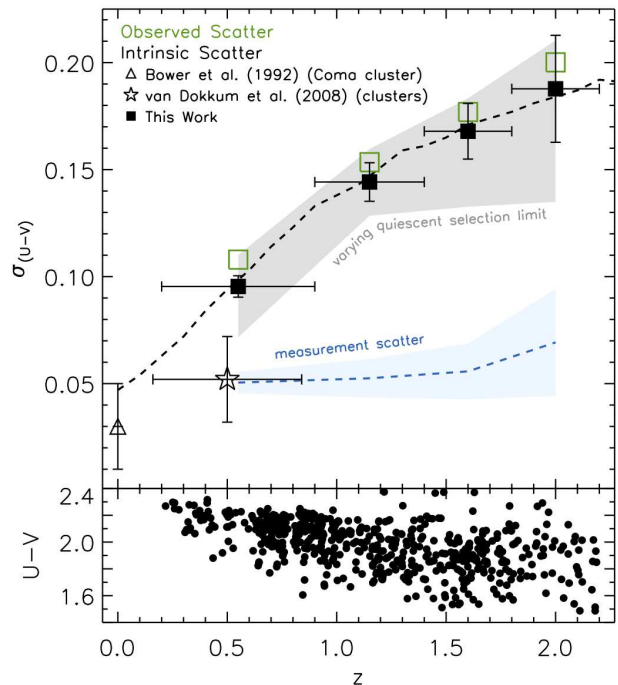


FIG. 3.— The observed (green) and intrinsic (black) scatter in the rest-frame $U-V$ colors of the most massive, quiescent galaxies selected by their extinction-correct $U-V$ colors. The scatter due to measurement errors (blue) is subtracted from the observed scatter in quadrature. The vertical black error bars mark the 68% confidence intervals due to photometric errors and the grey filled region indicates how σ_{U-V} changes when we raise and lower the horizontal selection limit in Figure 1 by ± 0.2 magnitudes. The dashed line is the expected evolution of the intrinsic scatter due to passive evolution for galaxies that started forming stars at $z=3$ with a characteristic timescale for transformation into an early-type galaxy of 1.4 Gyrs, with a large burst of star formation before transforming. The observed $U-V$ data points used to calculate the color scatter as a function of redshift are plotted in the bottom panel. We find that the scatter in $U-V$ increases towards higher redshift, where the intrinsic scatter is significantly higher than the scatter introduced by photometric and systematic errors at $z \sim 2$.

The age as defined in stellar populations models strongly depends on the choice of star formation history. To simplify, we assume an exponentially decaying star formation history with $\tau=0.1$ Gyr and $0 < A_V < 3$. Using the stellar population synthesis code FAST (Kriek et al. 2009) with the Maraston (2005) models and a Kroupa (2001) IMF, we fit for the age of these stellar populations given the above constraints. Given our assumptions, we effectively measure the relative ages (and dust) of the quiescent galaxies, fixing all other parameters.

Absolute ages may not be very meaningful given our modeling approach, but the relative ages of blue and red galaxies are robust if we assume that they have similar star formation histories. In Figure 4, we plot the best-fit age of all quiescent galaxies as a function of their rest-frame $U-V$ color. The reddest galaxies have systematically older stellar populations than the bluest galaxies at all redshifts. Given the assumption of solar metallicity, there exist a few quiescent galaxies consistent with the age of the universe (dotted horizontal lines) at $z \gtrsim 1$. We include the typical 68% confidence intervals in the ages in Figure 4 from the modeling described in §2, rather

than the modeling in §3.3, as the average uncertainty is much smaller than what we expect given our assumptions in the modeling due to degeneracies between age and metallicity. Additionally, we plot the typical random and systematic errors in the $U-V$ color as a function of redshift in Figure 4. At $z < 1.5$, the red and blue quartiles have the same low-level of dust reddening, whereas at $z > 1.5$ the red quiescent galaxies have ~ 0.2 magnitudes more extinction.

3.4. Rest-Frame SEDs of Quiescent Galaxies

We note that the general trends in Figure 4 do not prove that we are measuring age differences, as bluer $U-V$ colors will force a lower age in the fit, even if the range in $U-V$ is due to photometric scatter only (see Appendix B for more details on the effects of photometric scatter). In the previous section we just considered the $U-V$ colors, we will now investigate the shape of the full observed rest-frame SEDs of these galaxies to see if there is a fundamental difference between the reddest and bluest galaxies on the red sequence.

Stellar populations with ages of ~ 0.8 Gyr will have strong Balmer breaks at 3646\AA , whereas older populations will have pronounced 4000\AA breaks. Although the differences will be subtle, the SEDs of galaxies with ages of ~ 0.8 -1 Gyr should be distinct from older stellar populations. This has not been observed previously at high z because the J , H , and K broad-band filters smooth over these spectral features. Figure 5 demonstrates the importance of the spectral resolution by comparing the composite SED of the reddest quartile at $0.9 < z < 1.4$ (light grey points) to models smoothed to the resolution of the

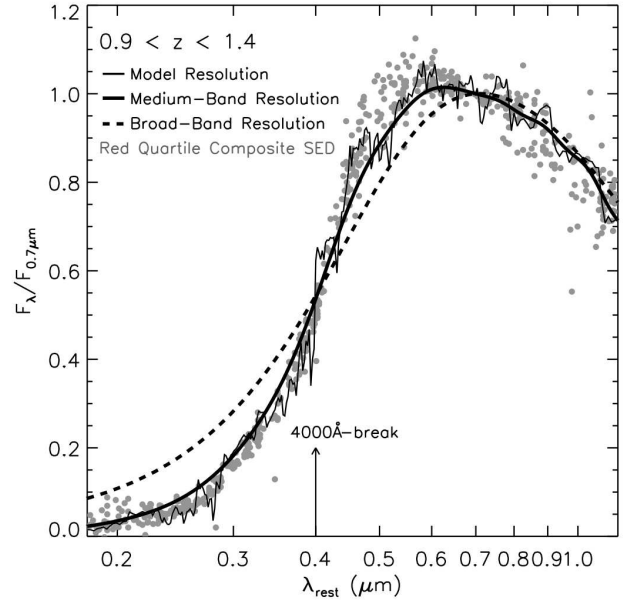


FIG. 5.— The effect of resolution can be seen in this figure, where the thin black line is the average best-fit model to the rest-frame composite SED from the medium-band measurements of 46 reddest galaxies over the redshift range $0.9 < z < 1.4$ (also shown in Figure 6). If this model is then smoothed with a Gaussian with a width equal to the resolution of the medium-band filters, $0.15\mu\text{m}/(1+z)$, we see that the smoothed model at medium-band resolution (thick black line) is smoother than the model at original resolution, but still follows the shape of the Balmer/ 4000\AA -break region closely. Note that we mark the location of the 4000\AA -break with an arrow. We then smooth the models with a Gaussian that has a width equal to the typical resolution of broad-band filters, $0.4\mu\text{m}/(1+z)$ (dashed line). The Balmer/ 4000\AA -break has become washed out due to the poor resolution.

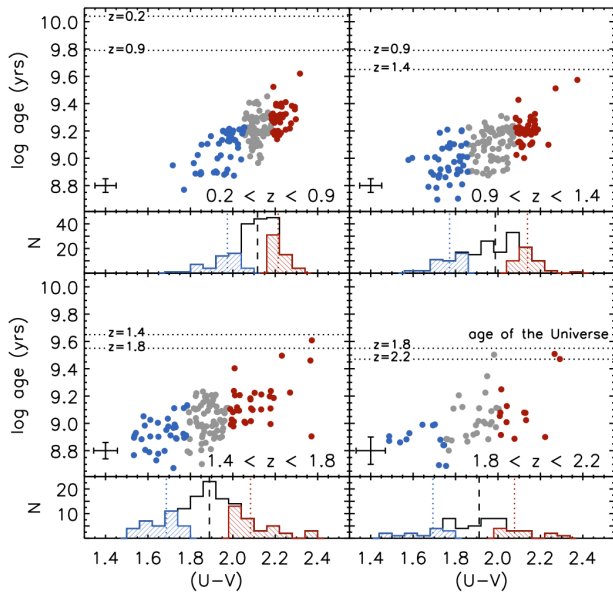


FIG. 4.— These panels contain the ages of quiescent galaxies (as derived from spectral synthesis models in §3.2) as a function of rest-frame $U-V$ color, in four redshift bins. The reddest and bluest $U-V$ quartiles are denoted by the colors red and blue, respectively, while the grey points are the middle quartiles. The dotted line signifies the maximum age of the universe within each redshift bin. The bottom panels contain histograms of colors, where the red and blue dotted lines in the bottom panels are the median colors of the two quartiles and the black, dashed line is the median color over the entire redshift interval. The general trend at all redshifts is that redder galaxies are typically older than bluer quiescent galaxies.

medium- and broad-band filters. For the first time, we are able to distinguish these features with the NMBS due to the increased sampling of the Balmer/ 4000\AA break region by the medium-band filters and the accurate photometric redshifts. We therefore consider the rest-frame SEDs of these quiescent galaxies to understand if the intrinsic scatter we measure is really due to the ages of the galaxies. Specifically, we are interested in the SEDs of the reddest and bluest quartiles (red and blue, respectively, in Figure 4). If the scatter is due to age as implied from the spectral synthesis modeling, we should see an increasing dichotomy in the SEDs of these quartiles as we look to higher z , where we observe an increasing internal scatter in color.

With the improved resolution and photometric redshift accuracies of the medium-band filters, we are able to measure the relative ages of a complete sample of massive galaxies inhabiting the red sequence out to $z \sim 2$ for the first time. The rest-frame SEDs of these massive galaxies are plotted in Figure 6, including all individual observed fluxes from u - $8\mu\text{m}$ shifted to the rest-frame for all quiescent galaxies, normalized at 7000\AA . We consider the SEDs of the reddest and bluest quartiles in $U-V$ (shown in the inset $U-V$ histograms), where the observed fluxes of the galaxies with the reddest colors are indicated with red points and the bluest galaxies with blue points. The median best-fit spectral synthesis model templates for the reddest and bluest quartiles are the solid lines in Figure 6, using the FAST settings as described in §3.3. The

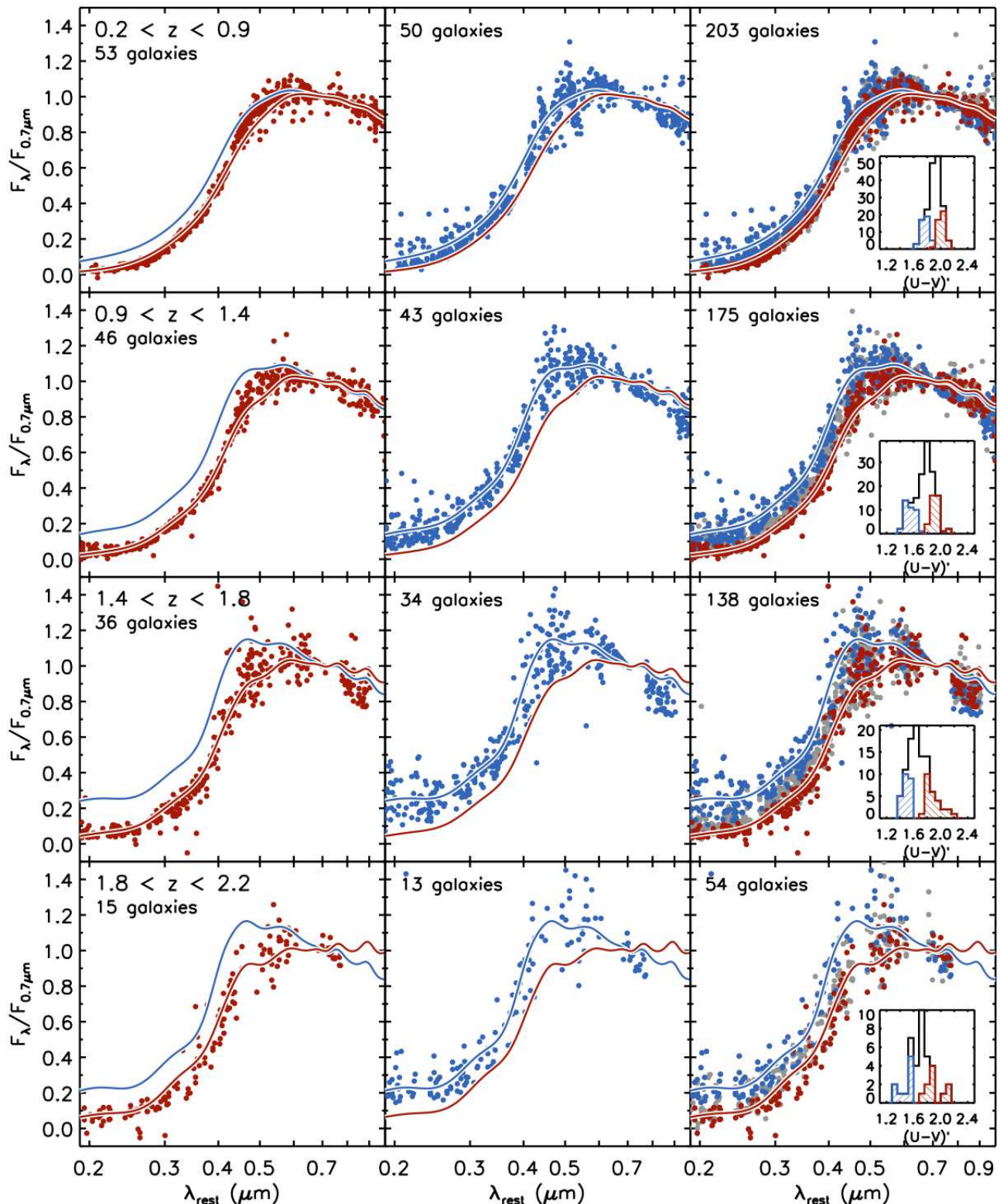


FIG. 6.— The composite rest-frame SED of massive, quiescent galaxies from $z=0.2$ to 2.2 in four redshift bins (top to bottom), with the reddest and bluest $U-V$ quartiles selected in Figure 4 color-coded the same. From left to right, we see the reddest composite SED, the bluest composite SED and finally the composite SED of all quiescent galaxies in grey with the two quartiles overplotted in the right panels. The solid lines are the median best-fit templates as derived from the spectral modeling analysis in §3.2, smoothed with a Gaussian with a width equal to the average rest-frame medium-band filter resolution of $0.15\mu\text{m}/(1+z)$. The redshift range is labeled in the top left for each bin, and the total number of galaxies in each panel is indicated in the top, left corner. The sub-panels in each redshift range on the right are the histograms of $(U-V)'$, $U-V$ with the slope of the color-magnitude relation removed. The spectral shapes of the reddest and bluest quartiles are very similar at low redshift. At high redshift, there exist old quiescent galaxies (red) and young quiescent galaxies (blue) that leads to a relatively large observed intrinsic scatter in $U-V$.

models are shown in Figure 6 with Gaussian smoothing by the average rest-frame distance between the medium-band filters of $\sim 0.15\mu\text{m}/(1+z)$. Notice that there is more smoothing at lower redshift (due to the dependence of the resolution on the scale factor) and we therefore expect to resolve the Balmer/4000Å-break region with higher resolution at high- z because the medium-band filters span a shorter wavelength range.

We see an increasing dichotomy between the SEDs of the reddest, oldest galaxies and the bluest, youngest galaxies relative to 7000Å with the increasing intrinsic scatter in color. The SEDs are not only different in $U-V$, which is how they are selected (and also template dependent), rather at *all* rest-frame wavelengths. Furthermore, we plot all observed fluxes for our sample of galaxies in the right panels of Figure 6 to demonstrate the robustness and fundamental differences between the reddest and bluest galaxies on the red sequence. The remaining 50% of the sample that have intermediate $U-V$ colors (grey points) bridge the gap between the SEDs of the reddest and bluest quartiles at $z\sim 2$. With the composite rest-frame SEDs, we sample the Balmer/4000Å break region with sufficient resolution to distinguish between a Balmer- or 4000Å-break. We note that the models do not fit the lowest redshift galaxies very well, tending to force slightly larger differences between the quadrants at $0.4 < \lambda_{\text{rest}} < 0.6\mu\text{m}$ than observed. As a test, we have included different metallicities in the modeling described in §3.3, and we find that they reduce the discrepancy between the best-fit model and data points seen for the reddest galaxies at $z \lesssim 1.5$ slightly, but not entirely.

In the high redshift bins, we see that the bluest, youngest galaxies emit more radiation than the reddest galaxies at all wavelengths $< 7000\text{Å}$. In particular, the region around $0.4\text{--}0.5\mu\text{m}$ and $\lesssim 0.3\mu\text{m}$ (blueward of the U -band) show clear differences between the red and blue quiescent galaxies. These galaxies that populate the blue tail of the distribution have younger ages and bluer colors at higher redshifts. Focusing on the rest-frame UV wavelength regime, we see a factor of >2 increase in the continuum emission for the blue quartile with increasing redshift. Additionally, we see the flux in the Balmer break region grow in strength with increasing redshift.

While the SEDs of the bluest galaxies undergo significant evolution from $z=0.2$ to 2.2 , the oldest galaxies remain virtually unchanged. The old galaxies inhabit a very small range of $U-V$ colors with uniform spectral shapes at all redshifts. The rest-frame UV continuum is very faint and the galaxies have strong (smoothed) 4000Å breaks. We conclude that the increase in the $U-V$ scatter is driven by an increase in the dispersion of spectral types; there is a significant population of younger, blue quiescent galaxies at $z\sim 2$ that are nearly absent by $z\sim 0.5$. The observed rest-frame SEDs confirm that the major driver of the intrinsic scatter in color of the red sequence is the scatter in age, as the stellar populations originate from varying epochs in the universe. In Appendix B, we show that our results are robust against severe underestimates of the photometric errors, and against large systematic redshift errors. Additionally, we test the effects of dust and ongoing star formation on the composite SEDs in Appendix D.

4. THE REDDEST GALAXIES AT $Z\sim 2$

Kriek et al. (2006) (hereafter K06) were the first to show that many massive high- z galaxies have no (strong) emission lines and have strong Balmer/4000Å breaks within their spectroscopic sample of 9 quiescent galaxies. The K06 sample of quiescent galaxies had relatively young ages of 0.5-1 Gyr. Perhaps the most striking feature of Figures 4 & 6 is that we see evidence for very old galaxies at $z\sim 2$ that seem to have more evolved stellar populations than the K06 sample, with higher M/L ratios.

Selection effects may explain why the K06 did not find the more evolved galaxies we observe with the NMBS. The K06 NIR spectroscopic survey selected targets from the MUSYC K -selected photometric catalog (Gawiser et al. 2006; Quadri et al. 2007), choosing galaxies with photometric redshifts of $z\sim 2.3$. The targets were selected to a limiting magnitude of 21.6 in AB magnitudes to ensure an adequate signal-to-noise ratio for the NIR spectra.

In order to illustrate the difference between a magnitude-limited sample and a mass-limited sample, in Figure 7 we show the binned $U-V$ colors and ages (as derived in §3.3) as a function of the total K -band magnitude for all quiescent galaxies with photometric redshifts between $z=1.8$ and 2.2 . Brighter galaxies tend to have bluer colors and younger ages. We also note that we are observing an inversion of the color-magnitude relation. In Figure 7, the dashed line is the median K -band magnitude of the 9 spectroscopically-confirmed quiescent galaxies from K06 and the dotted line is the limiting magnitude of the spectroscopic survey. Both limits have been increased by ~ 0.4 magnitudes to account for the difference in median redshift: $z\sim 2.3$ for K06 and $z\sim 2$ for our sample (assuming no evolution). The magnitude-limited sample would not include galaxies that lie in the hashed region, thereby biasing the sample against the reddest and oldest galaxies.

In §3.4, we showed that the spectral shapes of the reddest and bluest galaxies on the red sequence are fundamentally different at $z\sim 2$. We compare the SEDs of the spectroscopically-confirmed quiescent galaxies from K06 to our mass-selected sample in Figure 8. The median rest-frame spectra of the K06 sample of quiescent galaxies binned to low resolution (grey shaded region) and smoothed with a Gaussian to the medium-band resolution matches the median SED of the bluest quiescent galaxies in our sample.

We cannot exclude the possibility that the differences between the spectra arise because we are comparing the K06 sample to galaxies at a slightly lower redshift. Because the galaxies in the spectroscopic sample will have aged by ~ 0.4 Gyr between $\langle z \rangle = 2.3$ and 2 , we fit the K06 spectra with a τ -model using the settings described in §3.3 finding a best-fit age of 0.8 Gyr, and age this best-fit model by $+0.4$ Gyr (black line in Figure 8). The median, aged K06 spectra lies roughly between the two extremes of our sample, which implies that typical $z=2$ galaxies could be descendants of the $z\sim 2.3$ galaxies of K06. It will be interesting to see whether very old galaxies exist at $z\sim 2.5$ and beyond.

Figures 7 and 8 illustrate the differences between mass-limited and magnitude-limited samples. Although a sim-

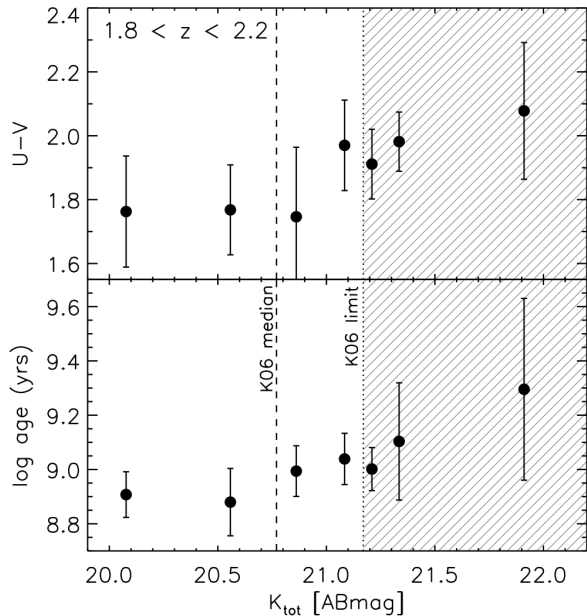


FIG. 7.— The binned $U-V$ color and ages of all quiescent galaxies as a function of their total K -band magnitudes. The dashed line is the median K -band magnitude of the 9 spectroscopically-confirmed quiescent galaxies by (Kriek et al. 2006) and the dotted line is the limiting magnitude used by Kriek et al. to select their sample. The reddest and oldest galaxies in the hashed region would therefore not be included in the Kriek et al. magnitude-limited sample.

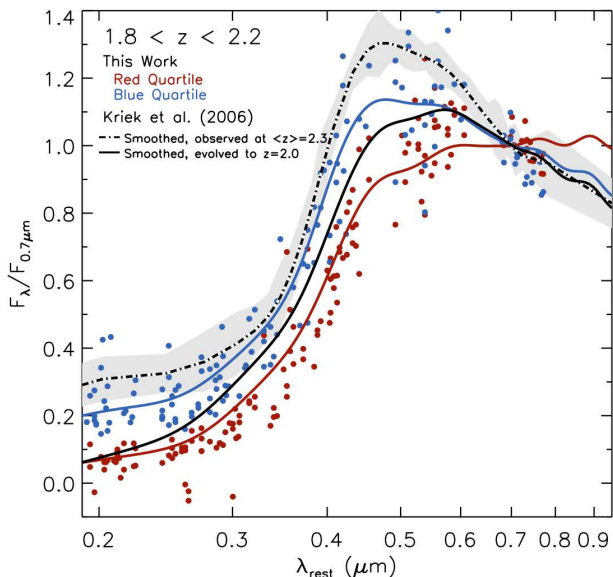


FIG. 8.— The composite rest-frame SED of the reddest and bluest $U-V$ quartiles of massive, quiescent galaxies from $z=1.8$ to 2.2 (red and blue points). The solid lines are the median best-fit templates as derived from the spectral modeling analysis with Gaussian smoothing to the medium-band resolution of $0.15\mu\text{m}/(1+z)$, compared to the median binned spectra of 9 quiescent galaxies at $z\sim 2.3$ from Kriek et al. (2006) (dot-dashed line, also smoothed to the medium-band resolution). The Kriek et al. sample match the spectral shape of the blue quartile. We also fit the Kriek et al. median spectra with a τ -model (see §4) and aged this best-fit model of 0.8 Gyr by +0.4 Gyr to evolve the spectra to the average redshift of the medium-band data of $z\sim 2$ (black line). The median, aged K06 spectra lies roughly between the extremes of our sample, which implies that typical $z\sim 2$ quiescent galaxies may be the descendants of the K06 sample.

ple magnitude limit is practical, one must be aware of the ways in which the limit can introduce biases into the galaxy sample. With our complete, mass-limited sample, we are able to quantify the build up of the massive end of the red sequence by using our observations to constrain models.

5. BUILD UP OF THE RED SEQUENCE

Given the observed evolution in the $U-V$ scatter and the trends with age, we next look to simple models to explain the build up of the red sequence. In Figure 9, we see that the fraction of massive galaxies with intrinsically red colors due to evolved stellar populations increases with time. At higher redshift, there is an increasing fraction of massive galaxies that are dusty and star forming, inhabiting the region close to the green valley in the CMR. About 90% of the most massive galaxies are quiescent at $z < 1$. We note that our sample of massive galaxies is selected with a fixed mass limit of $10^{11} M_{\odot}$ at all redshifts and will therefore not account for mass evolution. To test how sensitive the fractions are to the adopted mass limit, we also select a sample of massive galaxies at a constant number density of $n = 2 \times 10^{-4} \text{ Mpc}^{-3}$ following van Dokkum et al. (2010). The resulting fraction of quiescent and active galaxies is nearly identical to the fractions for a fixed mass limit. The uncertainty in the fraction of quiescent galaxies due mass evolution are indicated with the error bars in Figure 9. We also show the range of fractions that result when the selection limit (in Figure 1) is varied by ± 0.2 magnitudes (grey filled region).

Our results are consistent with many high redshift studies, which have found a significant fraction of quiescent galaxies in place at $z > 2$ (e.g. Fontana et al. 2009; Williams et al. 2009). We find that the most massive objects at $z=1.5-2$ are divided roughly equally between star forming and quiescent galaxies, the same results as Williams et al. (2009) and Fontana et al. (2009). Consistent with previous work (e.g. Kriek et al. 2008; Damen et al. 2009; Fontana et al. 2009), we find that the massive, quiescent galaxies observed at $z\sim 2$ assembled most of their stellar mass at higher redshifts.

The observed evolution of the fraction of quiescent galaxies and the color scatter can constrain simple passive evolution models with “progenitor bias”¹⁵. The Passive Evolution Calculator¹⁶ (van Dokkum & Franx 2001) models the evolution with three parameters: t_{start} , τ_{stop} and f_{\star} . The parameter t_{start} is the time when star formation starts and the parameter τ_{stop} is the characteristic scale for the probability distribution of the times when star formation stops. The variation of the star formation rate is accounted for with the dimensionless parameter f_{\star} ; the star formation history can include bursts and increasing or decreasing continuous formation rates as a function of time. Once the star formation is quenched in galaxies, the luminosity and color evolution is well approximated by a single-age population of stars with the same luminosity-weighted mean age (see van Dokkum &

¹⁵ At high z , young early-type galaxies will drop out of samples creating a biased subset of the low z sample that contains only the oldest progenitors of today’s early-types. This effect is known as “progenitor bias” and leads to an underestimate of the observed redshift evolution of the mean luminosity and colors of early-types.

¹⁶ <http://www.astro.yale.edu/dokkum/old.index.html>

Franx 2001). The parameter f_* can range between 0 and 1; the limiting case of $f_* \sim 0$ implies that most of the stars formed close to the start of star formation, $f_* \sim 0.5$ is a roughly constant star formation history and when $f_* \sim 1$, the luminosity-weighted mean age of the stellar populations is dominated by a burst at the end of the star formation history. These models can be applied to observations of early-type galaxies, enabling fits to the early-type galaxy fraction, the mean color evolution and the scatter in the CMR¹⁷.

Here, we use the Passive Evolution Calculator to predict the redshift evolution of $U-V$, the rms scatter in $U-V$ and the fraction of today's early-types that are in place by redshift z for early-type galaxies that started forming stars at $z=3$. We assume the timescale for transformation to quiescent galaxies is zero (in other words, the truncation of star formation is instantaneous) and vary the probability distribution of stop times for transformation from star forming galaxy to quiescent galaxy, τ_{stop} , and the form of the star formation history of the individual galaxies, f_* . By matching the predicted intrinsic scatter in $U-V$ to the observed scatter, we find a best-fit characteristic timescale for transformation of $\tau_{\text{stop}} = 1.4_{-0.5}^{+0.3}$ Gyrs and a luminosity weighted formation time of the stars of $f_* = 0.92_{-0.05}^{+0.03}$. The best-fit model broadly reproduces the observed scatter in Figure 3 and the early-type fraction in Figure 9, although the fit is not particularly good at high redshift.

The resulting best-fit values result in low values of τ_{stop} , which implies that the most massive early-type

galaxies mainly formed at high redshift. This result is consistent with Marchesini et al. (2009), who find that there is very little evolution in the number density of the most massive galaxies from $z \sim 4$ to 1.5, pointing towards a high formation redshift for the most massive galaxies in the universe. Furthermore, the relatively high values of f_* indicate that these galaxies experienced a burst of star formation close to the end of the period of star formation. These results indicate that massive, dusty galaxies with high star formation rates may be the progenitors of the most massive quiescent early-type galaxies. According to this simple model, about $\sim 20\%$ of the massive, dusty star forming galaxies at $z \sim 2$ have specific star formation rates $> 1 \text{ Gyr}^{-1}$. This reservoir of massive dusty star-forming galaxies will likely soon quench and migrate to the red sequence at lower redshifts.

The evolution of the red sequence may involve more complicated processes beyond simple passive evolution. For example, we see that the observed fraction of quiescent galaxies evolves more strongly beyond $z \sim 1.5$ in Figure 9, the same epoch where the color evolution seems to be inconsistent with passive evolution. The predicted evolution of the early-type fraction from passive evolution (dashed line in Figure 9) is less steep than the observed evolution at $z \gtrsim 1.5$. Using a very similar selection of galaxies from the NMBS, van Dokkum et al. (2010) calculate that the star formation rate drops by a factor of 20 from $z=2$ to $z=1.1$, whereas the stellar mass grows only by a factor of 1.4 in the same redshift interval. This rapid evolution implies that more complicated processes may govern the quenching of star formation. Additionally, once galaxies have moved to the red sequence there may still be other physical mechanisms acting aside from simple passive evolution.

We plot the mean $U-V$ color as a function of redshift in Figure 10 and compare this with the predictions from the models, which are forced to agree with the mean $U-V$ color at $z=0.5$. It is interesting that there is no evolution in color between $z=2$ and 1.6, as this implies that this epoch is where the red sequence is most heavily supplemented with newly quenched galaxies. Although the σ_{U-V} and early-type fractions appear consistent with passively evolving galaxies with a range of truncation times at $z \lesssim 1.5$, the observed color evolution is clearly inconsistent. Even the most extreme case of the color evolution of a single stellar population (SSP) formed at a redshift of infinity is inconsistent with the $z \sim 2$ mean color. The grey filled region shows the selection effect of changing the color limit by ± 0.2 magnitudes. Reducing the lower boundary of the $U-V$ color selection will result in a bluer mean color at $z \sim 2$, but it cannot reconcile the difference between the data and the best-fit model from the color scatter (although the extreme case of a SSP formed at $z = \infty$ does agree for the lowest magnitude selection limit only). This discrepancy between the observed color evolution and the predictions from passive evolution has been noted in other studies (e.g. Kriek et al. 2008), and there are several mechanisms that may slow the color evolution of galaxies. Galaxies may be dustier at higher redshift, which will redden the intrinsic colors. A visual extinction of $\sim 0.2-0.3$ (which would be consistent with the observed SEDs) will redden the $U-V$ color by ~ 0.1 mag, which is similar to the offset we see at $z \sim 1-1.5$ between our observed color and that predicted

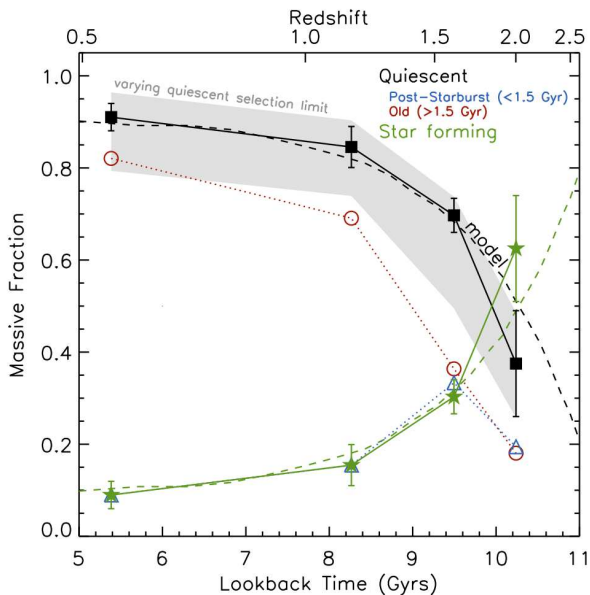


FIG. 9.— The fraction of massive galaxies ($>10^{11} M_{\odot}$) that are quiescent (black squares) and still star forming (green stars). Additionally, the quiescent galaxies are broken down by those old galaxies that have stellar populations >1.5 Gyr (red circles) and those that are younger with ages <1.5 Gyr (blue triangles), as derived from the SED modeling described in §2. The black dashed line is the expected evolution of the fraction of early-type galaxies from passive evolution given the observed scatter in $U-V$. At $z \sim 1.5-2$, roughly half of the most massive galaxies are quiescent.

¹⁷ The parameter Δt in van Dokkum & Franx 2001 is set to zero, as we are not concerned with the time when a galaxy is morphologically identified as early-type.

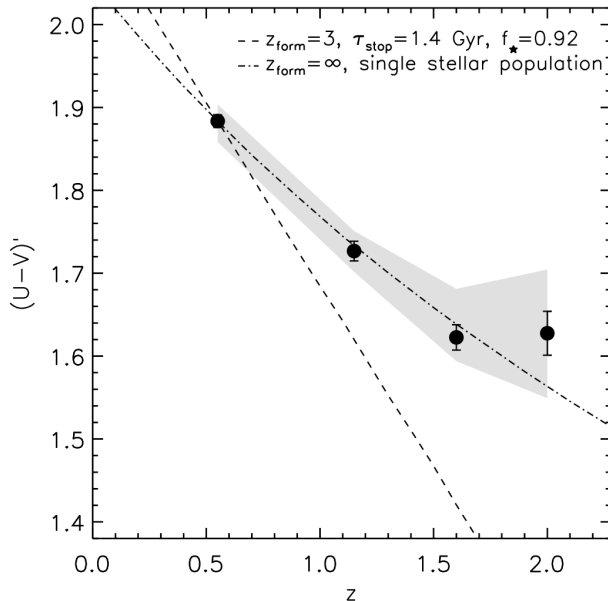


FIG. 10.— The mean rest-frame color with the slope of the CMR removed, $(U-V)'$, as a function of redshift. The color evolution from simple passive evolution models that include growth of the red sequence by transformation of blue galaxies predict too strong a color evolution, especially the best-fit model to the color scatter (dashed line). The color evolution of a single stellar population forming at infinity (dashed-dot line) disagrees at high redshift, where the mean color flattens between $z \sim 1.5-2$. Other mechanisms such as dust, dry mergers or “frostings” of young stars may be important to slow the color evolution.

from passive evolution given the observed color scatter (dashed line in Figure 10). The median visual extinction, A_V , from the spectral synthesis modeling described in §2 of the quiescent galaxies in our sample is 0.3 mag. Regardless, Kriek et al. (2008) find that dust does not provide a solution as the absolute color evolution for solar metallicity shows that the $z \sim 2$ galaxies are not too red, rather the $z \sim 0$ galaxies are too blue. We note that in this paper we simply normalize the colors at $z=0.5$ and do not consider the absolute values. We explore the effects of dusts on the spectral shapes in more detail in Appendix D, finding that dust may be a secondary effect on the composite SEDs in Figure 6.

In addition to dust extinction, a plausible mechanism to weaken the color evolution of these quiescent galaxies includes recent low level bursts of star formation. If these galaxies have experienced a recent burst of star formation, a frosting of young stars should be evident in the SEDs of these galaxies. The continuum shape would appear to be a composite of an old stellar population with a strong 4000Å break and a young component visible in the rest-frame UV. We see some evidence for this amongst a fraction of these quiescent galaxies; roughly 10% of the highest redshift galaxies have negative slopes in the rest-frame UV, parameterized by $F_\lambda \propto \lambda^\beta$. However, a frosting of young stars may be too transient a feature to effect the mean color evolution. We test how ongoing star formation would effect the composite SEDs in Appendix D, finding that a more complex star formation history cannot reproduce the trends of spectral shape with $U-V$ color.

Following the work of Kriek et al. (2008), another pos-

sible mechanism that would slow the color evolution of quiescent galaxies is red mergers. With deep observations of a sample of nearby bulge-dominated early-type galaxies, van Dokkum (2005) and Tal et al. (2009) find morphological signatures of tidal interactions and infer that red mergers may lead to a factor $\gtrsim 2$ evolution in the stellar mass density of luminous red galaxies at $z < 1$. Red (dry) major mergers of two red sequence galaxies will shift the galaxies towards higher masses for the same color and ages. While the mean ages of the stellar populations are unchanged, red mergers will therefore slow the color evolution and probably become significant at $z \lesssim 1-1.5$. It is unclear what the dominant mechanism is that slows the color evolution of red sequence galaxies, perhaps all of the methods described above are important at different epochs.

6. SUMMARY AND CONCLUSIONS

In this work, we have selected a complete, mass-selected sample of quiescent galaxies out to $z=2.2$ through a selection based on extinction corrections to the $U-V$ colors (Brammer et al. 2009). We first demonstrate that we can measure accurate rest-frame colors at $z=1-2$ using the medium-band filters. We find that the intrinsic scatter in the rest-frame $U-V$ color of quiescent galaxies increases with redshift, measuring a scatter that is $\gtrsim 2$ times larger than previous cluster measurements at $z \sim 0.5$ (see Table 1 for a data summary). This measurement implies a potential real difference between the evolution of the scatter in the field and in the cluster environment. If confirmed, this may suggest that quiescent cluster galaxies are older than quiescent field galaxies, although the difference would be somewhat larger than found previously from the fundamental plane (see §3.2). The scatter can be explained by trends of $U-V$ with the relative ages of the stellar populations. Those galaxies with intrinsically redder $U-V$ colors have older stellar populations than those galaxies in the blue tail of the distribution. To bolster the argument, we show the composite rest-frame SEDs for all galaxies in the sample. The rest-frame SEDs highlight the usefulness of the NIR medium-bandwidth filters in sampling the Balmer/4000Å-break region at a higher resolution than the tradition broadband filters. The observed SEDs show a very clear trend of an emerging spread between quiescent red, old galaxies and quiescent blue, younger quiescent galaxies that exists up to and beyond $z \sim 2$.

The main result from our paper is that we find both young and old quiescent galaxies at $z \sim 2$, leading to a relatively large scatter in the $U-V$ colors of massive, quiescent galaxies at these redshifts. The presence of a large population of young, quiescent galaxies implies that galaxies were strongly forming stars shortly before star formation ended. As shown in §5, parameterizing the star formation history by f_* , which describes the luminosity weighted formation time of the stars for a model that includes progenitor bias and passive evolution, we find $f_* = 0.92^{+0.03}_{-0.05}$. This star formation history predicts massive galaxies with high sSFRs, which are seen at $z \sim 2$ in Figure 1. We suspect that these massive, star-forming galaxies at $z \sim 2$ are the progenitors of massive galaxies at lower redshifts and a few may possibly be detected as sub-mm sources.

TABLE 1
DATA RESULTS SUMMARY

Redshift	Number of Galaxies	Observed Scatter σ_{U-V} (mag)	Measurement Scatter σ_{U-V} (mag)	Intrinsic Scatter σ_{U-V} (mag)	Mean $(U-V)'$	Quiescent Fraction
$0.2 < z < 0.9$	203	0.108	0.050	0.095	1.883	0.91
$0.9 < z < 1.4$	175	0.153	0.052	0.144	1.726	0.85
$1.4 < z < 1.8$	138	0.178	0.056	0.168	1.623	0.70
$1.8 < z < 2.2$	54	0.200	0.069	0.188	1.628	0.38

The significant population of old galaxies at $z \sim 2$ pushes back the star formation epoch of the oldest massive galaxies. Galaxies with dominant 4000Å breaks (not post-starburst) comprise $\sim 20\%$ of the total population of massive galaxies at $z \sim 2$. It is interesting to speculate whether the $z=7-8$ star-forming galaxies that have been found recently in the Hubble Ultra-Deep Field (Bouwens et al. 2009; Oesch et al. 2010) could be the progenitors of these galaxies. Their stellar masses are $10^9-10^{10} M_{\odot}$ (Labbé et al. 2010), which may imply that substantial growth would be necessary between $z=6$ and $z=2$. It may also be that more massive galaxies exist than have been found so far in the fields studied at these high redshifts.

Using our high quality SED modeling (including optical through IR photometry, medium-band NIR photometry and accurate photometric redshifts), we find galaxies that appear to be nearly the age of the universe, even at these high redshifts. The oldest galaxies observed in this study may have been under-represented in the spectroscopic studies of red sequence galaxies at $z \sim 2.3$ by Kriek et al. (2006, 2008). Kriek et al. draw their targets from a larger sample of galaxies selected to a limiting K-band magnitude of 21.6 in the AB magnitude system. Because they use a magnitude limit, they may have missed the oldest galaxies in the universe. However, deep follow-up spectroscopy of one quiescent galaxy shows that this galaxy, which was initially classified as a post-starburst system, was actually much older and dominated by a 4000Å break (Kriek et al. 2009). Although we have good reason to believe this galaxy is not representative of the full sample (see Kriek et al. 2009), this case illustrates that caution is required. It is also possible that the differences with the Kriek et al. sample may simply be due to the slightly different mean redshifts. In any case, this work highlights the importance of un-

derstanding how a simple magnitude limit can introduce biases into a galaxy sample. With increasing numbers of high-quality surveys becoming public, it is important to select samples to some limiting mass to probe the full range of properties of galaxies.

Future studies combining the NMBS with *HST* WFC3 imaging will enable more detailed studies of the sizes and morphologies of the most massive galaxies at high redshift. It would be interesting if there exists a relationship between $U-V$ and the size of these galaxies, where the reddest quiescent galaxies may also be the most compact. Or perhaps the earliest compact, quiescent galaxies may have had time to grow through mergers between $z \sim 3$ and 2 and are therefore larger than the recently “quenched” galaxies (Mancini et al. 2010). Whatever the case may be, size measurements of this sample of quiescent galaxies will provide constraints on galaxy evolution scenarios linking the known compact, quiescent systems at high redshift (e.g. Trujillo et al. 2006; van Dokkum et al. 2008; Cimatti et al. 2008) to the early-type galaxies in the local universe.

We thank the anonymous referee for useful comments and a careful reading of the paper. This paper is based partly on observations obtained with MegaPrime/MegaCam, a joint project of CFHT and CEA/DAPNIA, at the Canada-France-Hawaii Telescope (CFHT), which is operated by the National Research Council (NRC) of Canada, the Institut National des Science de l’Univers of the Centre National de la Recherche Scientifique (CNRS) of France, and the University of Hawaii. We thank H. Hildebrandt for providing the CARS-reduced CFHT-LS images. Support from NSF grants AST-0449678 and AST-0807974 is gratefully acknowledged.

facilities: Mayall (NEWMIR)

REFERENCES

- Barmby, P., Huang, J., Ashby, M. L. N., Eisenhardt, P. R. M., Fazio, G. G., Willner, S. P., & Wright, E. L. 2008, *ApJS*, 177, 431
- Bell, E. F., McIntosh, D. H., Barden, M., Wolf, C., Caldwell, J. A. R., Rix, H., Beckwith, S. V. W., Borch, A., Häussler, B., Jahnke, K., Jogee, S., Meisenheimer, K., Peng, C., Sanchez, S. F., Somerville, R. S., & Wisotzki, L. 2004a, *ApJ*, 600, L11
- Bell, E. F., Wolf, C., Meisenheimer, K., Rix, H., Borch, A., Dye, S., Kleinheinrich, M., Wisotzki, L., & McIntosh, D. H. 2004b, *ApJ*, 608, 752
- Bertin, E., & Arnouts, S. 1996, *A&AS*, 117, 393
- Bouwens, R. J., Illingworth, G. D., Labbe, I., Oesch, P. A., Carollo, M., Trenti, M., van Dokkum, P. G., Franx, M., Stiavelli, M., Gonzalez, V., & Magee, D. 2009, *ArXiv e-prints*
- Bower, R. G., Lucey, J. R., & Ellis, R. S. 1992, *MNRAS*, 254, 601
- Brammer, G. B., van Dokkum, P. G., & Coppi, P. 2008, *ApJ*, 686, 1503
- Brammer, G. B., Whitaker, K. E., van Dokkum, P. G., Marchesini, D., Labbé, I., Franx, M., Kriek, M., Quadri, R. F., Illingworth, G., Lee, K., Muzzin, A., & Rudnick, G. 2009, *ApJ*, 706, L173
- Calzetti, D., Armus, L., Bohlin, R. C., Kinney, A. L., Koornneef, J., & Storchi-Bergmann, T. 2000, *ApJ*, 533, 682
- Capak, P., Aussel, H., Ajiki, M., McCracken, H. J., Mobasher, B., Scoville, N., Shopbell, P., Taniguchi, Y., Thompson, D., Tribiano, S., Sasaki, S., Blain, A. W., Brusa, M., Carilli, C., Comastri, A., Carollo, C. M., Cassata, P., Colbert, J., Ellis, R. S., Elvis, M., Giavalisco, M., Green, W., Guzzo, L., Hasinger, G., Ilbert, O., Impey, C., Jahnke, K., Kartaltepe, J., Kneib, J., Koda, J., Koekemoer, A., Komiyama, Y., Leauthaud, A., Lefevre, O., Lilly, S., Liu, C., Massey, R., Miyazaki, S., Murayama, T., Nagao, T., Peacock, J. A., Pickles, A., Porciani, C., Renzini, A., Rhodes, J., Rich, M., Salvato, M., Sanders, D. B., Scarlata, C., Schiminovich, D., Schinnerer, E., Scodreggio, M., Sheth, K., Shioya, Y., Tasca, L. A. M., Taylor, J. E., Yan, L., & Zamorani, G. 2007, *ApJS*, 172, 99
- Cimatti, A., Cassata, P., Pozzetti, L., Kurk, J., Mignoli, M., Renzini, A., Daddi, E., Bolzonella, M., Brusa, M., Rodighiero, G., Dickinson, M., Franceschini, A., Zamorani, G., Berta, S., Rosati, P., & Halliday, C. 2008, *A&A*, 482, 21
- Cowie, L. L., & Barger, A. J. 2008, *ApJ*, 686, 72

- Daddi, E., Dickinson, M., Morrison, G., Chary, R., Cimatti, A., Elbaz, D., Frayer, D., Renzini, A., Pope, A., Alexander, D. M., Bauer, F. E., Giavalisco, M., Huynh, M., Kurk, J., & Mignoli, M. 2007, *ApJ*, 670, 156
- Daddi, E., Renzini, A., Pirzkal, N., Cimatti, A., Malhotra, S., Stiavelli, M., Xu, C., Pasquali, A., Rhoads, J. E., Brusa, M., di Serego Alghieri, S., Ferguson, H. C., Koekemoer, A. M., Moustakas, L. A., Panagia, N., & Windhorst, R. A. 2005, *ApJ*, 626, 680
- Damen, M., Labbé, I., Franx, M., van Dokkum, P. G., Taylor, E. N., & Gawiser, E. J. 2009, *ApJ*, 690, 937
- Davis, M., Faber, S. M., Newman, J., Phillips, A. C., Ellis, R. S., Steidel, C. C., Conselice, C., Coil, A. L., Finkbeiner, D. P., Koo, D. C., Guhathakurta, P., Weiner, B., Schiavon, R., Willmer, C., Kaiser, N., Luppino, G. A., Wirth, G., Connolly, A., Eisenhardt, P., Cooper, M., & Gerke, B. 2003, in *Society of Photo-Optical Instrumentation Engineers (SPIE) Conference Series*, Vol. 4834, *Society of Photo-Optical Instrumentation Engineers (SPIE) Conference Series*, ed. P. Guhathakurta, 161–172
- Ellis, R. S., Smail, I., Dressler, A., Couch, W. J., Oemler, Jr., A., Butcher, H., & Sharples, R. M. 1997, *ApJ*, 483, 582
- Erben, T., Hildebrandt, H., Lerchster, M., Hudelot, P., Benjamin, J., van Waerbeke, L., Schrabback, T., Brimiouille, F., Cordes, O., Dietrich, J. P., Holhjem, K., Schirmer, M., & Schneider, P. 2009, *A&A*, 493, 1197
- Fontana, A., Santini, P., Grazian, A., Pentericci, L., Fiore, F., Castellano, M., Giallongo, E., Menci, N., Salimbeni, S., Cristiani, S., Nonino, M., & Vanzella, E. 2009, *A&A*, 501, 15
- Franx, M., van Dokkum, P. G., Schreiber, N. M. F., Wuyts, S., Labbé, I., & Toft, S. 2008, *ApJ*, 688, 770
- Gallazzi, A., Charlot, S., Brinchmann, J., & White, S. D. M. 2006, *MNRAS*, 370, 1106
- Gawiser, E., van Dokkum, P. G., Herrera, D., Maza, J., Castander, F. J., Infante, L., Lira, P., Quadri, R., Toner, R., Treister, E., Urry, C. M., Altmann, M., Assef, R., Christlein, D., Coppi, P. S., Durán, M. F., Franx, M., Galaz, G., Huerta, L., Liu, C., López, S., Méndez, R., Moore, D. C., Rubio, M., Ruiz, M. T., Toft, S., & Yi, S. K. 2006, *ApJS*, 162, 1
- Hildebrandt, H., Pielorz, J., Erben, T., van Waerbeke, L., Simon, P., & Capak, P. 2009, *A&A*, 498, 725
- Hilton, M., Stanford, S. A., Stott, J. P., Collins, C. A., Hoyle, B., Davidson, M., Hosmer, M., Kay, S. T., Liddle, A. R., Lloyd-Davies, E., Mann, R. G., Mehrtens, N., Miller, C. J., Nichol, R. C., Romer, A. K., Sabirli, K., Sahlén, M., Viana, P. T. P., West, M. J., Barbary, K., Dawson, K. S., Meyers, J., Perlmutter, S., Rubin, D., & Suzuki, N. 2009, *ApJ*, 697, 436
- Holden, B. P., Stanford, S. A., Eisenhardt, P., & Dickinson, M. 2004, *AJ*, 127, 2484
- Kriek, M., van der Wel, A., van Dokkum, P. G., Franx, M., & Illingworth, G. D. 2008, *ApJ*, 682, 896
- Kriek, M., van Dokkum, P. G., Franx, M., Quadri, R., Gawiser, E., Herrera, D., Illingworth, G. D., Labbé, I., Lira, P., Marchesini, D., Rix, H., Rudnick, G., Taylor, E. N., Toft, S., Urry, C. M., & Wuyts, S. 2006, *ApJ*, 649, L71
- Kriek, M., van Dokkum, P. G., Labbé, I., Franx, M., Illingworth, G. D., Marchesini, D., & Quadri, R. F. 2009, *ApJ*, 700, 221
- Kroupa, P. 2001, *MNRAS*, 322, 231
- Labbé, I., Franx, M., Rudnick, G., Schreiber, N. M. F., Rix, H., Moorwood, A., van Dokkum, P. G., van der Werf, P., Röttgering, H., van Starckenburg, L., van de Wel, A., Kuijken, K., & Daddi, E. 2003, *AJ*, 125, 1107
- Labbé, I., González, V., Bouwens, R. J., Illingworth, G. D., Oesch, P. A., van Dokkum, P. G., Carollo, C. M., Franx, M., Stiavelli, M., Trenti, M., Magee, D., & Kriek, M. 2010, *ApJ*, 708, L26
- Labbé, I., Huang, J., Franx, M., Rudnick, G., Barmby, P., Daddi, E., van Dokkum, P. G., Fazio, G. G., Schreiber, N. M. F., Moorwood, A. F. M., Rix, H., Röttgering, H., Trujillo, I., & van der Werf, P. 2005, *ApJ*, 624, L81
- Lidman, C., Rosati, P., Tanaka, M., Strazzullo, V., Demarco, R., Mullis, C., Ageorges, N., Kissler-Patig, M., Petr-Gotzens, M. G., & Selman, F. 2008, *A&A*, 489, 981
- Lilly, S. J., Le Fèvre, O., Renzini, A., Zamorani, G., Scodreggio, M., Contini, T., Carollo, C. M., Hasinger, G., Kneib, J., Iovino, A., Le Brun, V., Maier, C., Maimieri, V., Mignoli, M., Silverman, J., Tasca, L. A. M., Bolzonella, M., Bongiorno, A., Bottini, D., Capak, P., Caputi, K., Cimatti, A., Cucciati, O., Daddi, E., Feldmann, R., Franzetti, P., Garilli, B., Guzzo, L., Ilbert, O., Kampezyk, P., Kovac, K., Lamareille, F., Leauthaud, A., Borgne, J., McCracken, H. J., Marinoni, C., Pello, R., Ricciardelli, E., Scarlata, C., Vergani, D., Sanders, D. B., Schinnerer, E., Scoville, N., Taniguchi, Y., Arnouts, S., Aussel, H., Bardelli, S., Brusa, M., Cappi, A., Ciliegi, P., Finoguenov, A., Foucaud, S., Franceschini, R., Halliday, C., Impey, C., Knobel, C., Koekemoer, A., Kurk, J., Maccagni, D., Maddox, S., Marano, B., Marconi, G., Meneux, B., Mobasher, B., Moreau, C., Peacock, J. A. R., Porciani, C., Pozzetti, L., Scaramella, R., Schiminovich, D., Shopbell, P., Smail, I., Thompson, D., Tresse, L., Vettolani, G., Zanichelli, A., & Zucca, E. 2007, *ApJS*, 172, 70
- Maíz Apellániz, J. 2006, *AJ*, 131, 1184
- Mancini, C., Daddi, E., Renzini, A., Salmi, F., McCracken, H. J., Cimatti, A., Onodera, M., Salvato, M., Koekemoer, A. M., Aussel, H., Floc'h, E. L., Willott, C., & Capak, P. 2010, *MNRAS*, 401, 933
- Maraston, C. 2005, *MNRAS*, 362, 799
- Marchesini, D., van Dokkum, P. G., Förster Schreiber, N. M., Franx, M., Labbé, I., & Wuyts, S. 2009, *ApJ*, 701, 1765
- McIntosh, D. H., Bell, E. F., Rix, H., Wolf, C., Heymans, C., Peng, C. Y., Somerville, R. S., Barden, M., Beckwith, S. V. W., Borch, A., Caldwell, J. A. R., Häußler, B., Jahnke, K., Jee, S., Meisenheimer, K., Sánchez, S. F., & Wisotzki, L. 2005a, *ApJ*, 632, 191
- McIntosh, D. H., Zabludoff, A. I., Rix, H., & Caldwell, N. 2005b, *ApJ*, 619, 193
- Mei, S., Holden, B. P., Blakeslee, J. P., Ford, H. C., Franx, M., Homeier, N. L., Illingworth, G. D., Jee, M. J., Overzier, R., Postman, M., Rosati, P., Van der Wel, A., & Bartlett, J. G. 2009, *ApJ*, 690, 42
- Muzzin, A., Marchesini, D., van Dokkum, P. G., Labbé, I., Kriek, M., & Franx, M. 2009, *ApJ*, 701, 1839
- Oesch, P. A., Bouwens, R. J., Illingworth, G. D., Carollo, C. M., Franx, M., Labbé, I., Magee, D., Stiavelli, M., Trenti, M., & van Dokkum, P. G. 2010, *ApJ*, 709, L16
- Papovich, C., Dickinson, M., Giavalisco, M., Conselice, C. J., & Ferguson, H. C. 2005, *ApJ*, 631, 101
- Papovich, C., Momcheva, I., Willmer, C. N. A., Finkelstein, K. D., Finkelstein, S. L., Tran, K., Brodwin, M., Dunlop, J. S., Farrah, D., Khan, S. A., Lotz, J., McCarthy, P., McLure, R. J., Rieke, M., Rudnick, G., Sivanandam, S., Pacaud, F., & Pierre, M. 2010, *ArXiv e-prints*
- Quadri, R., Marchesini, D., van Dokkum, P., Gawiser, E., Franx, M., Lira, P., Rudnick, G., Urry, C. M., Maza, J., Kriek, M., Barrientos, L. F., Blanc, G. A., Castander, F. J., Christlein, D., Coppi, P. S., Hall, P. B., Herrera, D., Infante, L., Taylor, E. N., Treister, E., & Willis, J. P. 2007, *AJ*, 134, 1103
- Quadri, R. F., & Williams, R. J. 2009, *ArXiv e-prints*
- Romeo, A. D., Napolitano, N. R., Covone, G., Sommer-Larsen, J., Antonuccio-Delogu, V., & Capaccioli, M. 2008, *MNRAS*, 389, 13
- Ruhland, C., Bell, E. F., Häußler, B., Taylor, E. N., Barden, M., & McIntosh, D. H. 2009, *ApJ*, 695, 1058
- Sanders, D. B., Salvato, M., Aussel, H., Ilbert, O., Scoville, N., Surace, J. A., Frayer, D. T., Sheth, K., Helou, G., Brooke, T., Bhattacharya, B., Yan, L., Kartaltepe, J. S., Barnes, J. E., Blain, A. W., Calzetti, D., Capak, P., Carilli, C., Carollo, C. M., Comastri, A., Daddi, E., Ellis, R. S., Elvis, M., Fall, S. M., Franceschini, A., Giavalisco, M., Hasinger, G., Impey, C., Koekemoer, A., Le Fèvre, O., Lilly, S., Liu, M. C., McCracken, H. J., Mobasher, B., Renzini, A., Rich, M., Schinnerer, E., Shopbell, P. L., Taniguchi, Y., Thompson, D. J., Urry, C. M., & Williams, J. P. 2007, *ApJS*, 172, 86
- Steidel, C. C., Adelberger, K. L., Shapley, A. E., Pettini, M., Dickinson, M., & Giavalisco, M. 2003, *ApJ*, 592, 728
- Tal, T., van Dokkum, P. G., Nelan, J., & Bezanson, R. 2009, *AJ*, 138, 1417
- Trujillo, I., Förster Schreiber, N. M., Rudnick, G., Barden, M., Franx, M., Rix, H., Caldwell, J. A. R., McIntosh, D. H., Toft, S., Häußler, B., Zirm, A., van Dokkum, P. G., Labbé, I., Moorwood, A., Röttgering, H., van der Werf, A., van der Werf, P., & van Starckenburg, L. 2006, *ApJ*, 650, 18
- van Dokkum, P. G. 2005, *AJ*, 130, 2647
- 2008, *ApJ*, 674, 29
- van Dokkum, P. G., & Franx, M. 2001, *ApJ*, 553, 90
- van Dokkum, P. G., Franx, M., Fabricant, D., Illingworth, G. D., & Kelson, D. D. 2000, *ApJ*, 541, 95
- van Dokkum, P. G., Franx, M., Kelson, D. D., Illingworth, G. D., Fisher, D., & Fabricant, D. 1998, *ApJ*, 500, 714

van Dokkum, P. G., Franx, M., Kriek, M., Holden, B., Illingworth, G. D., Magee, D., Bouwens, R., Marchesini, D., Quadri, R., Rudnick, G., Taylor, E. N., & Toft, S. 2008, *ApJ*, 677, L5
 van Dokkum, P. G., Labbé, I., Marchesini, D., Quadri, R., Brammer, G., Whitaker, K. E., Kriek, M., Franx, M., Rudnick, G., Illingworth, G., Lee, K., & Muzzin, A. 2009, *PASP*, 121, 2
 van Dokkum, P. G., & van der Marel, R. P. 2007, *ApJ*, 655, 30
 van Dokkum, P. G., Whitaker, K. E., Brammer, G., Franx, M., Kriek, M., Labbé, I., Marchesini, D., Quadri, R., Bezanson, R., Illingworth, G. D., Muzzin, A., Rudnick, G., Tal, T., & Wake, D. 2010, *ApJ*, 709, 1018
 Williams, R. J., Quadri, R. F., Franx, M., van Dokkum, P., & Labbé, I. 2009, *ApJ*, 691, 1879

Wolf, C., Gray, M. E., & Meisenheimer, K. 2005, *A&A*, 443, 435
 Wolf, C., Meisenheimer, K., Rix, H., Borch, A., Dye, S., & Kleinheinrich, M. 2003, *A&A*, 401, 73
 Wuyts, S., Labbé, I., Franx, M., Rudnick, G., van Dokkum, P. G., Fazio, G. G., Förster Schreiber, N. M., Huang, J., Moorwood, A. F. M., Rix, H., Röttgering, H., & van der Werf, P. 2007, *ApJ*, 655, 51
 Wyder, T. K., Martin, D. C., Schiminovich, D., Seibert, M., Budavári, T., Treyer, M. A., Barlow, T. A., Forster, K., Friedman, P. G., Morrissey, P., Neff, S. G., Small, T., Bianchi, L., Donas, J., Heckman, T. M., Lee, Y., Madore, B. F., Milliard, B., Rich, R. M., Szalay, A. S., Welsh, B. Y., & Yi, S. K. 2007, *ApJS*, 173, 293

APPENDIX A. UVJ SELECTION OF QUIESCENT GALAXIES

In this paper we select galaxies based on their extinction-corrected $U-V$ colors. We show here that this selection method is similar to a selection based on the rest-frame $U-V$ and $V-J$ colors used by Labbé et al. (2005) and Williams et al. (2009). This alternative color-selection has been shown to cleanly separate quiescent and star-forming galaxies. Two distinct populations exist in the $U-V$ versus $V-J$ color-space; the red, quiescent galaxies tend to lie in a clump, while the star-forming galaxies follow a well-separated track that extends from blue to red $U-V$ colors with increasing amounts of dust extinction.

We applied the same selection method as used in Williams et al. (2009) to separate the star forming and quiescent galaxies, independent of the method used in this paper. The resulting sample of massive, quiescent galaxies are very similar, the fraction of quiescent galaxies agree within 5% at all redshifts. In Figure 11a, the massive, quiescent galaxies do indeed cleanly separate from star forming galaxies in the UVJ color-color plot. A few of the quiescent galaxies selected in the UVJ method have large amounts of dust reddening, as seen in Figure 11b by plotting the extinction-corrected $U-V$ colors as a function of mass. These blue quiescent galaxies will increase the measured intrinsic scatter at high redshift while making the mean color at these redshifts bluer by $\sim 0.2-0.4$ mag.

We have repeated the analysis as described in §3 for this new sample of quiescent galaxies. In Figure 12, we show that the measured intrinsic scatter of the UVJ sample of quiescent galaxies rises even more steeply at $z > 1$. These trends in the color scatter imply even shorter characteristic timescales for star formation as well as luminosity-weighted ages that are dominated by star formation close to the end of their star formation histories. This may be due to contamination by star-forming galaxies; whatever the cause, we note that our selection is more conservative

In Figure 13, we show the composite rest-frame SED of the UVJ -selected sample of quiescent galaxies, derived using the same method as described in §3.4. Comparing the distribution of colors from the UVJ -selection criterion to the histograms in the inset panels of Figure 7, we see that the galaxies selected here extend to bluer $U-V$ colors and have broader distributions. We also see that the bluest quiescent galaxies from this selection method show stronger rest-frame UV emission and there is a more pronounced clump of blue points that lie above the model around 5000-6000Å in the highest redshift bin. This may be evidence for emission lines in these blue galaxies. Emission lines are

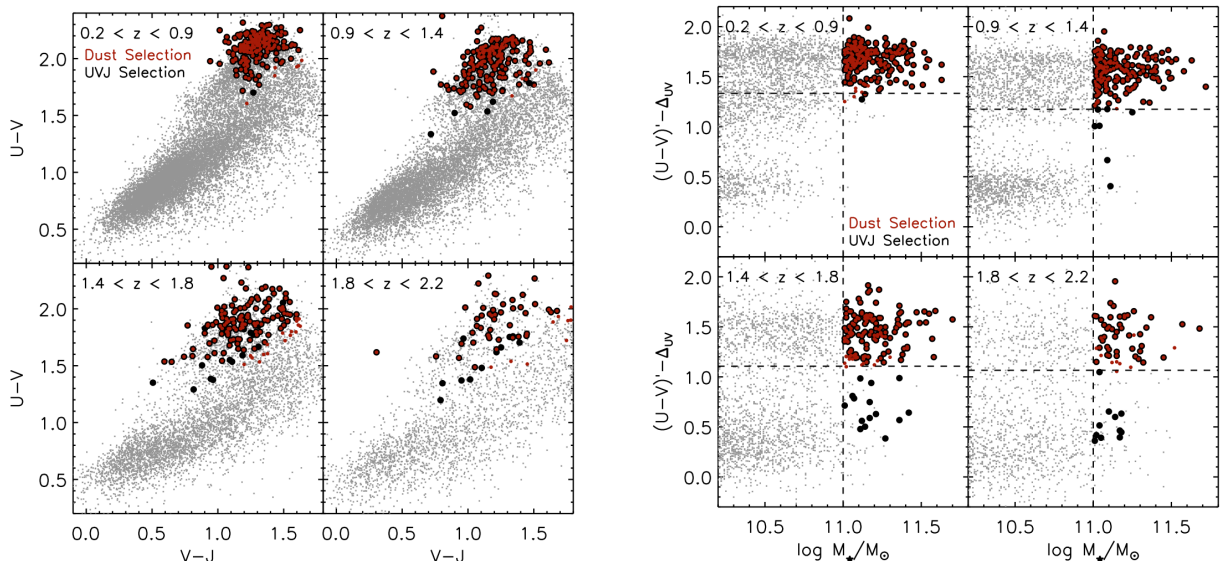


FIG. 11.— (Left) The $U-V$ versus $V-J$ color-color diagram for all galaxies in the NMBS sample (greyscale). Those galaxies that are both massive ($>10^{11} M_{\odot}$) and have rest-frame $U-V$ colors within the selection-window of Williams et al. (2009) are show as black, filled circles and those galaxies that are selected based on their $U-V$ colors corrected for dust reddening in this paper are red, filled circles. (Right) The color-mass diagram for all galaxies in the NMBS sample (greyscale) with the quiescent sample that would be selected following the UVJ -method of Williams et al. (2009) in black and the dust extinction corrected color selection in red.

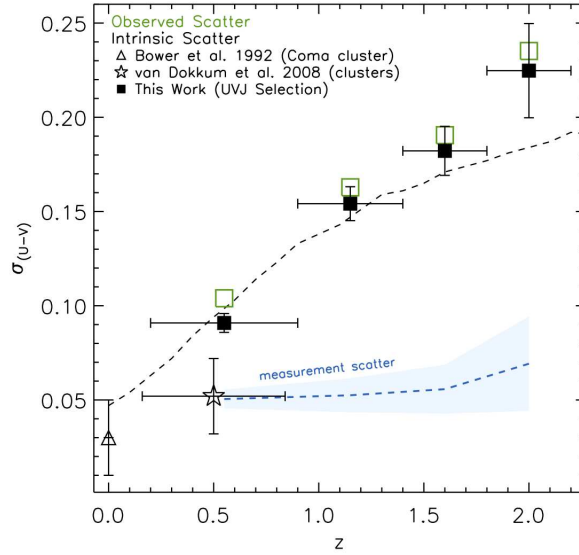


FIG. 12.— The observed (green) and intrinsic (black) scatter in the rest-frame $U-V$ colors of the most massive, quiescent galaxies selected by their $U-V$ and $V-J$ colors. The scatter due to measurement errors (blue) is removed from the observed scatter. The vertical black error bars mark the 68% confidence intervals due to photometric errors and the larger green error bars are systematic errors due to the selection method. The dashed line is the expected evolution of the intrinsic scatter due to passive evolution for galaxies that started forming stars at $z=3$ with a characteristic timescale for transformation into an early-type galaxy of 1.4 Gyrs, with a large burst of star formation before transforming.

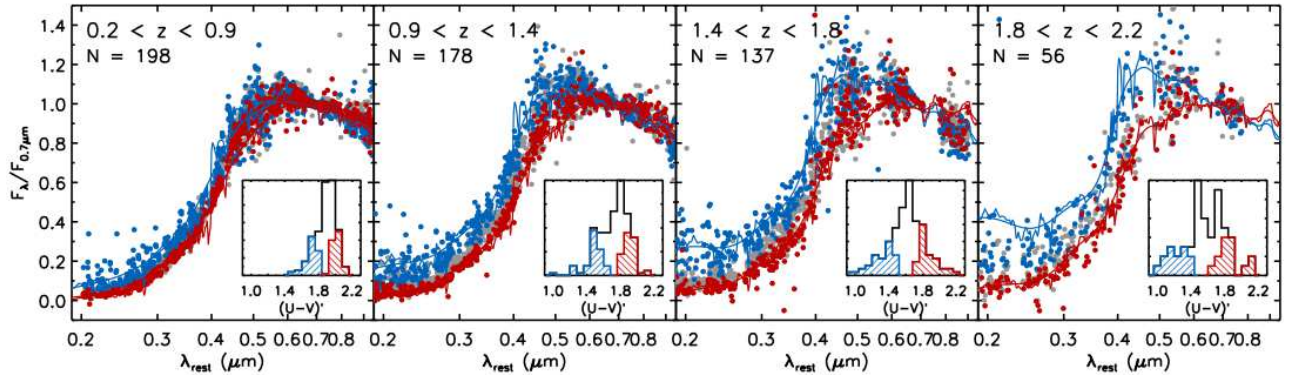


FIG. 13.— The composite rest-frame SED of massive, quiescent galaxies from $z=0.2$ to 2.2 , selected based on their $U-V$ and $V-J$ colors. The reddest and bluest $U-V$ quartiles are color-coded as red and blue, and the solid lines are the median best-fit templates as derived from the spectral modeling analysis. The sub-panels in each redshift range are the histograms of $(U-V)'$, $U-V$ with the slope of the color-magnitude relation removed. The total number of galaxies in each bin is labeled in the top left of each panel. There is an even larger difference between the composite SEDs of the red and blue quartiles at $z \sim 2$, compared to our more conservative sample in Figure 6.

generally too weak to affect the SED modeling, although their signal is (just) strong enough to identify in the average, de-redshifted spectrum of star-forming galaxies with the NMBS (Brammer et al. *in prep*). These quiescent galaxies with even bluer colors that enter the sample at $z \sim 2$ are the massive galaxies just below our selection limit. Most of these galaxies also have MIPS detections and may therefore have some recent star formation or host AGN. In general, our selection based on the extinction-corrected $U-V$ colors is in fact more conservative than a UVJ -selection.

In summary, a selection of quiescent galaxies based on their $U-V$ and $V-J$ colors yields a very similar sample of galaxies. Both methods result in the same fundamental differences between the reddest and bluest quiescent galaxies.

APPENDIX B. THE EFFECTS OF PHOTOMETRIC SCATTER

We consider what the rest-frame SEDs would look like if the scatter in color was in fact due solely to photometric errors of a single age population. We find the median SED for all quiescent galaxies in the highest redshift bin and use this template to derive what the observed flux would be if these galaxies all had the same age but a range of redshifts between $1.8 < z < 2.2$. Next we perturb the fluxes by increasing factors of the observed error bars and re-measure the rest-frame colors until the scatter in the rest-frame $U-V$ color matches our observed scatter of $\sigma_{U-V} \sim 0.15-0.17$. The error bars have to be increased by a factor of 8 to yield an observed scatter consistent with our observations.

Although it is doubtful that our photometric errors are underestimated by a factor of 8, we plot the SEDs of all simulated fluxes for a single-age stellar population (black model) with scatter that results from the increased

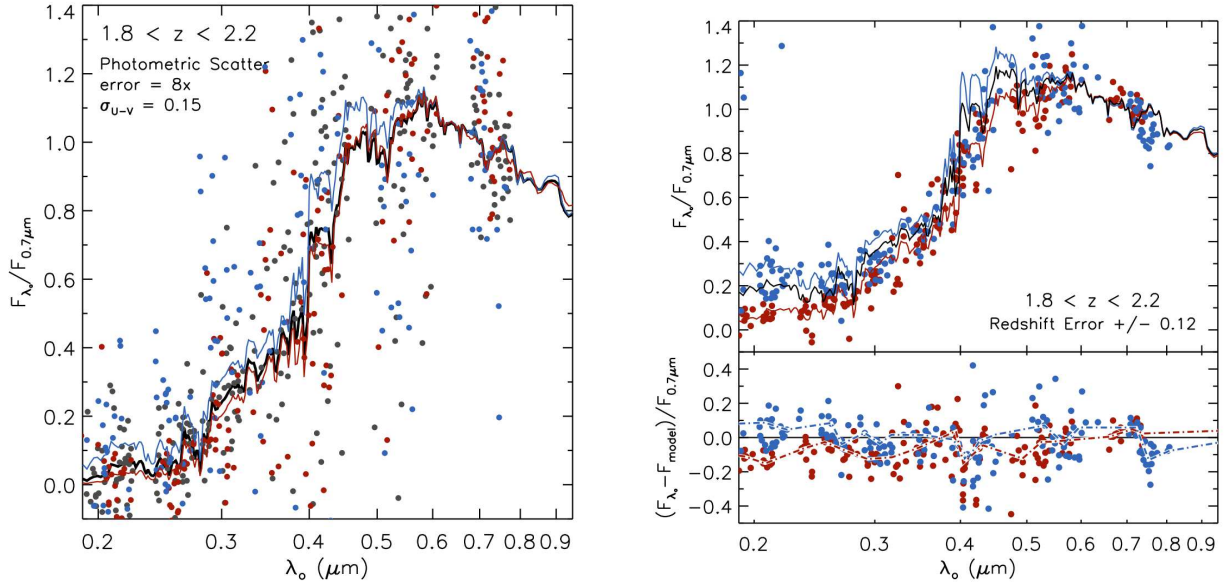


FIG. 14.— (Left) Simulated fluxes of a single age stellar population (black model) with scatter due solely to photometric errors. The error bars had to be scaled up by a factor of 8 to measure a scatter in $U-V$ comparable to our results. The red and blue models are the median spectral synthesis models of the composite rest-frame SED shown here as points. The reddest and bluest quartiles in $U-V$ are the red and blue points, respectively.

FIG. 15.— (Right) The composite rest-frame SEDs of the red and blue quartiles at $1.8 < z < 2.2$, systematically offsetting the photometric redshifts by $\Delta z = \pm 0.12$, thereby shifting the blue stack to longer wavelengths and the red stack to shorter wavelengths (top panel). The black model is the average best-fit model from the blue and red quartiles. The residuals of the observed fluxes with respect to the average model is shown in the bottom panel, with the running median for each quartile shown as a dot-dashed line.

photometric errors in Figure 14 to see if we find similar trends to Figure 8. We plot all simulated fluxes and indicate those galaxies with the reddest $U-V$ colors in red and those with the bluest $U-V$ colors in blue, exactly as we have done in Figure 8. We see that the median best-fit spectral synthesis model for the bluest quartile does emit slightly more radiation at all wavelengths than the reddest quartile blueward of 7000\AA (as we have selected them). Although the models are well-behaved, the important result is that the observed fluxes are incoherent. These simulations show that the trends we observe cannot be the result of photometric errors alone.

Another concern is that the photometric redshifts suffer from both random and systematic errors. To understand the effects of random uncertainties in the photometric redshifts on the composite SEDs, we perturbed the redshifts of all quiescent galaxies in the highest redshift bin by their 68% confidence level uncertainties and re-fit the photometry. Although some scatter is introduced to the SEDs, we still find that the reddest galaxies emit systematically lower flux than the bluest galaxies on the red sequence at all wavelengths $< 7000\text{\AA}$. Although our results hold strong against random uncertainties in the photometric redshifts, systematic uncertainties may have a more severe effect.

Recently, Kriek et al. (2009) took a follow-up deep 30-hour spectra of a massive quiescent galaxy and derived a spectroscopic redshift of $z_{\text{spec}} = 2.186$. This galaxy was selected from the original sample of 9 quiescent galaxies from Kriek et al. (2006), where the spectroscopic redshift with a 6-hour integration was $z_{\text{spec}} = 2.31$. The error in z_{spec} of 0.12 in redshift space shifted the 4000\AA break to shorter wavelengths resulting in a continuum shape that appeared to instead have a strong Balmer-break and therefore a younger stellar population. If the photometric redshifts of the blue quiescent galaxies have been systematically under-estimated and the photometric redshifts of the oldest galaxies have been systematically over-estimated, we could falsely produce the spread of ages found in this work. To test how systematic errors would change the results, we assumed that the photometric redshifts of the bluest quartile were all under-estimated by $\Delta z = 0.12$ and the reddest quartile were over-estimated by $\Delta z = 0.12$ and re-fit the models. For this extreme case, the residuals between the average model of all of the data and the two quartiles overlap in the Balmer/ 4000\AA break region, however the rest-frame UV and rest-frame NIR show clear differences (see Figure 15). If we relax the systematic shifts from $\Delta z = 0.12$ to 0.06, the residuals once again show a clear difference over the entire wavelength regime. Although we cannot rule out that systematic effects may significantly affect our results, our photometric redshift errors would need to conspire quite drastically to wash out the fundamental differences between the SEDs of the reddest and bluest galaxies on the red sequence.

APPENDIX C. THE EFFECTS OF TEMPLATE SETS ON THE PHOTOMETRIC REDSHIFTS AND REST-FRAME COLORS

In this section, we briefly discuss how the template sets used to fit photometric redshifts and rest-frame colors can have important systematic effects. The optimized template set used for the EAZY photometric redshift code contains 6 templates, which is large enough to span a broad range of galaxy colors, while minimizing color and redshift

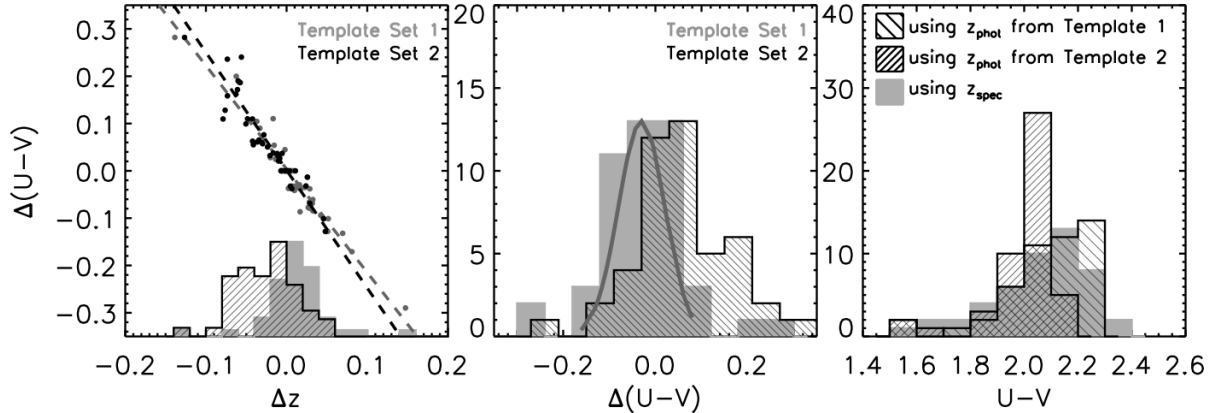


FIG. 16.— (Left) The difference in redshift ($z_{\text{spec}} - z_{\text{phot}}$) for photometric redshifts measured using Template Set 1 (which includes an additional old, red template, shown in grey) and Template Set 2 (the default set of EAZY templates, shown in black). The photometric redshifts of the reddest galaxies are systematically underestimated if the additional old template is not included. (Middle) The difference in measured rest-frame $U-V$ colors, $(U-V)_{\text{spec}} - (U-V)_{\text{phot}}$, as measured using the photometric redshifts from Template Set 1 (grey) and Template Set 2 (black). The systematic offset of ~ 0.05 in redshift space results in an offset of ~ 0.1 magnitudes in color when using Template Set 2. (Right) The $U-V$ distributions as measured from the spectroscopic redshifts (grey) and the photometric redshifts measured using Template Set 1 and 2. When the additional very old template is not included, the color distribution is artificially narrowed, and very peaked relative to the broader distribution of colors from the spectroscopic redshifts.

degeneracies. The default template set is described in detail in Brammer et al. (2008); the set includes 5 templates generated based on the PÉGASE models and calibrated with synthetic photometry from semi-analytic models, as well as an additional young and dusty template added to compensate for the lack of extremely dusty galaxies in semi-analytic models (we call this “Template Set 2” here). “Template Set 1”, which is the template set used in this paper, includes an additional template for a very old galaxy. This old, red template is from the Maraston (2005) models, with a Kroupa (2001) IMF and solar metallicity for a stellar population that has an age of 12.6 Gyrs.

Figure 16 shows how the additional old (red) template effects both the photometric redshifts measured as well as the $U-V$ colors. In the left panel, the difference between the spectroscopic and photometric redshifts is strongly correlated with the difference in the $U-V$ colors measured from these respective redshifts. The trend results in a systematic uncertainty in the $U-V$ color (as seen by the spread of the $\Delta(U-V)$ distribution in the middle panel) of 0.05 magnitudes¹⁸. In addition to this systematic uncertainty, there can be a systematic offset if the template set does not span the entire range of colors of the galaxies. In this case, Template Set 2 does not include a red enough template and therefore tends to over-estimate the photometric redshifts of the reddest galaxies (the black histogram in the left panel is offset). Furthermore, this over-estimate of the redshift leads to colors that are too blue (see the middle panel). Finally, if we compare the $U-V$ colors as measured from the spectroscopic redshifts and the photometric redshifts with the two template sets, we see that the color distribution is artificially peaked for Template Set 2. In other words, when the template set does not span the full range of galaxy colors, the scatter in color will be significantly underestimated.

APPENDIX D. THE EFFECTS OF DUST AND STAR FORMATION ON THE COMPOSITE SEDS

In §3.4, we concluded that the trends of spectral shape with the $U-V$ colors were mainly due to the spread in age of the quiescent galaxies. However, if the reddest galaxies are simply dustier versions of the bluest galaxies, we also might expect similar trends to result. Here we explore if the features we see in the composite SEDs in Figure 6 result not because the reddest quartile is older than the bluest quartile, but rather because the reddest galaxies are dustier. To test this, we take the smoothed best-fit model to the bluest quartile at $1.8 < z < 2.2$ and apply the Calzetti et al. (2000) dust extinction law to the spectrum with increasing amounts of dust to see if we can recover the shape of the reddest composite spectrum. From Figure 17, we see that for values of $A_V \sim 1.0$ mag match the data blueward of $0.4\mu\text{m}$, $A_V \sim 0.5$ mag matches the slope between $\sim 0.4-0.7\mu\text{m}$ and values of $A_V \sim 0.2$ mag agree with the IRAC data. There is no single extinction that is consistent over the full SED. We know that the red quiescent galaxies at $z > 1.5$ are ~ 0.2 magnitudes dustier on average than the blue quiescent galaxies, however it does not appear that the trends we see in Figure 6 can be explained by dust alone. With that said, we cannot rule out the possibility that dust has a second order effect on the trends of spectral shape with age.

Along the same lines, we suspect that some of these quiescent galaxies likely have ongoing star formation. The reddest quiescent galaxies probably have no recent star formation, whereas the bluest galaxies may have a more complicated star formation history that includes a recent burst of star formation. To understand how ongoing star-formation would effect the spectral shapes, we add Gaussian smoothed Maraston (2005) models with $\tau=0.1$ Gyr, Z_{\odot} , and a Kroupa (2001) IMF for a range of ages from 1 Myr to 0.4 Gyr to the composite SED of the reddest quartile. Recent star formation will have the largest contribution in the rest-frame UV, so we normalize these spectra to the observed flux

¹⁸ We note that the rest-frame $U-V$ color accuracy has a weak

dependence on mass and luminosity evolution, < 0.02 magnitudes.

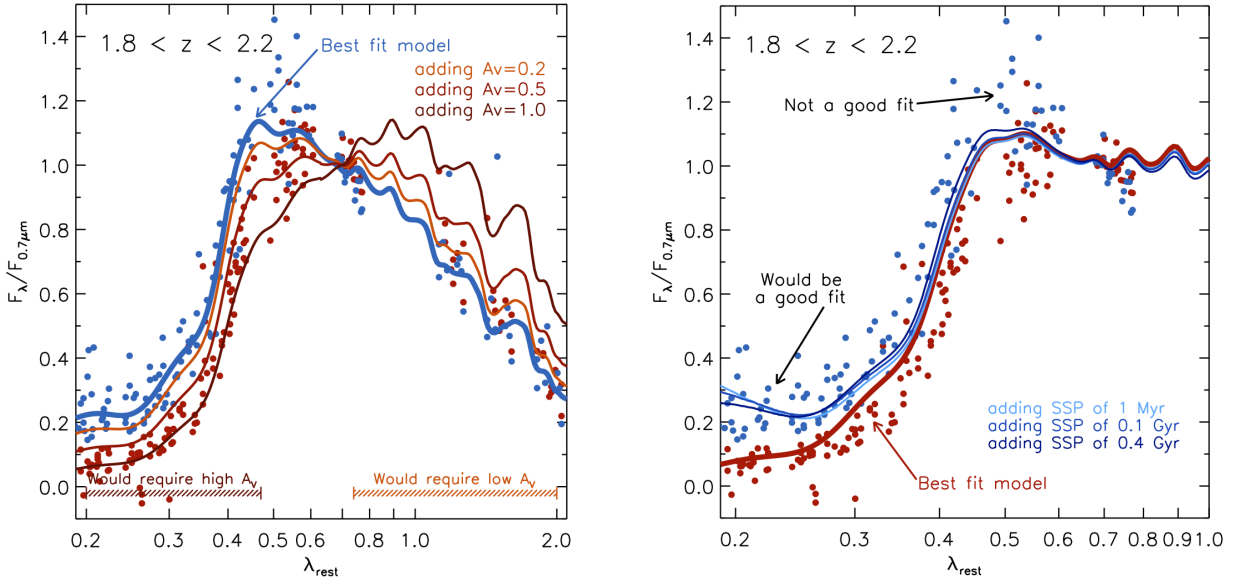


FIG. 17.— (Left) The effect of increasing levels of dust reddening on the blue composite SED, as compared to the red composite SED. No value of A_V matches the reddest composite SED over the entire wavelength range. Dust may have some contribution to the trends of Figure 6, but they are second order to the trends of $U-V$ with age.

FIG. 18.— (Right) The effect of ongoing star formation on the red composite SED, as compared to the blue composite SED. We add Gaussian smoothed Maraston (2005) models with $\tau=0.1$ Gyr, Z_{\odot} and a Kroupa (2001) IMF for ages of 0.001, 0.1 and 0.4 Gyr normalized at $0.2\mu\text{m}$ to the red composite SED, re-normalizing at $0.7\mu\text{m}$. A more complex star formation history does not result in a spectral shape similar to the blue composite SED; we are able to match the rest-frame UV of the bluest galaxies but not the Balmer-break region.

of the bluest quartile composite SED at $0.2\mu\text{m}$. We add a 0.001, 0.01, 0.1 and 0.4 Gyr stellar population to the reddest quartile composite spectrum and re-normalize the spectrum at 7000\AA . In Figure 18, we see that Balmer/4000Å-break region remains effectively unchanged regardless of the age of the young component we add to the red composite SED, while the slope in the rest-frame UV steadily rises blueward of $\sim 0.3\mu\text{m}$. From this simple analysis, we conclude that the difference between the blue and red composite SEDs cannot be the result of ongoing star formation in a subset of the quiescent galaxies. This does not mean that the quiescent galaxies have no ongoing star formation, rather that the trends we see in Figure 6 are not likely caused by more complex star formation histories.

APPENDIX E. THE EFFECTS OF METALLICITY VARIATIONS ON THE INTRINSIC $U-V$ SCATTER

In this paper, we assume that $U-V$ color scatter and variations in SED shapes are due to age variations between galaxies. However, metallicity variations could also contribute to the measured intrinsic scatter in $U-V$ color. Here we quantify this effect by using the Maraston (2005) models to predict how the $U-V$ scatter should evolve with redshift if the scatter is caused solely by metallicity variations (and not a spread in age). In the left panel of Figure 19, we see that red $U-V$ colors result from both older stellar populations and higher metallicities. Furthermore, the scatter in metallicity depends on the age of the stellar population. For ages $\gtrsim 3$ Gyr, the scatter in $U-V$ due to metallicity variations is roughly constant, with a smaller scatter for ages $\lesssim 3$ Gyr. The relation between $U-V$ and metallicity is shown in the middle panel of Figure 19, and is roughly linear with an age-dependent slope α . To characterize how the slope of the color-metallicity relation evolves with the age of the stellar population, we fit the $U-V$ color for 4 metallicities with a linear function and plot the slope as a function of the age in the right panel of Figure 19.

Given the evolution of the slope of the color-metallicity relation, we can predict how we expect the scatter in $U-V$ to evolve with redshift for a given scatter in metallicity. We first assume the age of the stellar population at $z=0$, which determines the slope of the color-metallicity relation from the right panel of Figure 19. We will further assume that $\sigma_{U-V} = 0.03$ at $z=0$, as determined in the Coma cluster (Bower et al. 1992). Given α and the scatter in $U-V$ at $z=0$, we can predict the scatter in $U-V$ due to $\log Z/Z_{\odot}$,

$$\sigma_{U-V}(z) = \frac{\sigma_{U-V}(z=0) \cdot \alpha(z=0)}{\alpha(z)} \quad (2)$$

The scatter due to metallicity, $\sigma_{U-V}(z=0) \cdot \alpha(z=0)$, is constant for a given age. However, the slope $\alpha(z)$ will change as the population evolves, leading to an evolving color scatter. In Figure 20, we find that the scatter in $U-V$ due to metallicity variations alone will stay roughly constant for the oldest stellar populations and eventually decrease. This trend in σ_{U-V} is opposite to the measured evolution of the intrinsic scatter in $U-V$ with redshift. We therefore expect that metallicity variations will not have a large effect on this work.

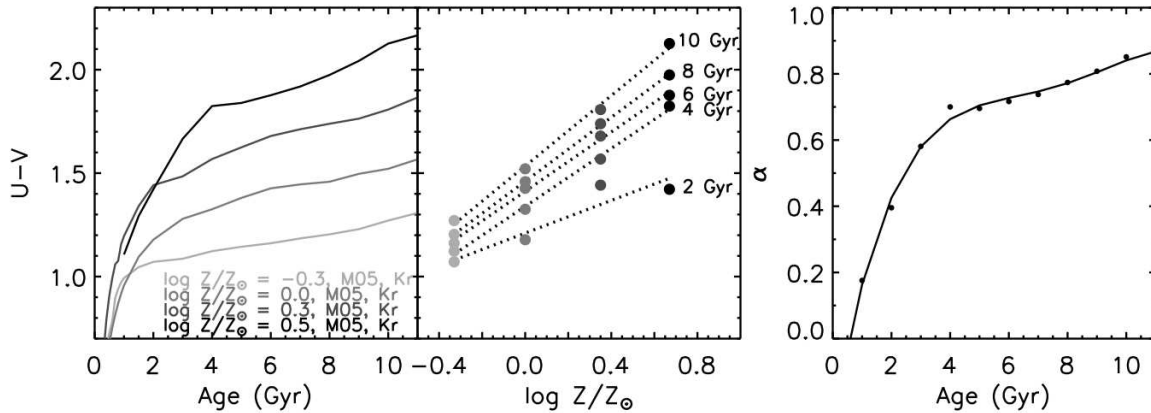


FIG. 19.— (Left) The $U-V$ color as a function of the age of the stellar population from the Maraston (2005) models for a range of metallicities. The $U-V$ colors are redder for higher metallicity and older stellar populations. The scatter in $U-V$ is roughly constant for stellar populations older than ~ 3 Gyr. (Middle) The $U-V$ color as a function of metallicity, from the Maraston (2005) models shown in the left panel. The points are fit linearly for 5 different ages (dotted lines), showing that the slope (α) increases with age. (Right) The slope of the relation between $U-V$ and metallicity as a function of the age of the stellar population.

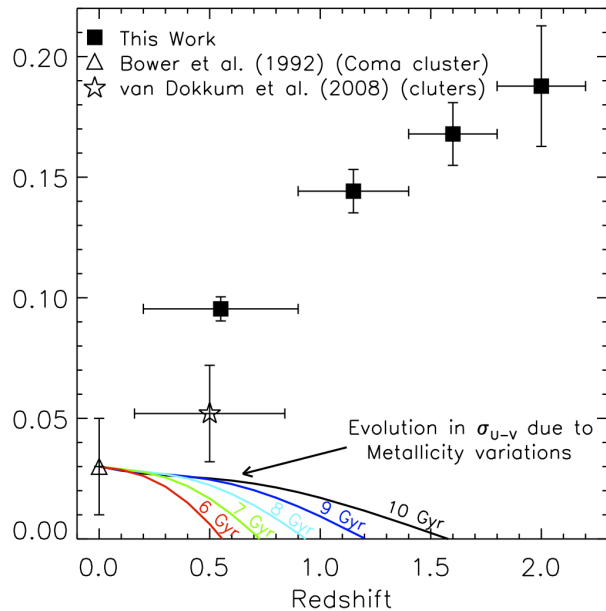


FIG. 20.— The intrinsic scatter in $U-V$ as a function of redshift as measured in clusters (Bower et al. 1992; van Dokkum 2008), as well as in this work. We compare the measured values to the expected evolution in σ_{U-V} if the color scatter is due solely to metallicity variations for a single aged stellar population. Metallicity variations will increase the scatter in $U-V$ for older ages and therefore lower redshifts, opposite to the trends found in this work.